Spontaneous curvature of bilayer membranes from molecular simulations: Asymmetric lipid densities and asymmetric adsorption

Bartosz Różycki[1,2] and Reinhard Lipowsky[1,a)]
[1]*Theory and Biosystems, Max Planck Institute of Colloids and Interfaces, 14424 Potsdam, Germany*
[2]*Institute of Physics, Polish Academy of Sciences, Al. Lotników 32/46, 02-668 Warsaw, Poland*

(Received 13 September 2014; accepted 24 December 2014; published online 2 February 2015)

Biomimetic and biological membranes consist of molecular bilayers with two leaflets which are typically exposed to different aqueous environments and may differ in their molecular density or composition. Because of these asymmetries, the membranes prefer to curve in a certain manner as quantitatively described by their spontaneous curvature. Here, we study such asymmetric membranes via coarse-grained molecular dynamics simulations. We consider two mechanisms for the generation of spontaneous curvature: (i) different lipid densities within the two leaflets and (ii) leaflets exposed to different concentrations of adsorbing particles. We focus on membranes that experience no mechanical tension and describe two methods to compute the spontaneous curvature. The first method is based on the detailed structure of the bilayer's stress profile which can hardly be measured experimentally. The other method starts from the intuitive view that the bilayer represents a thin fluid film bounded by two interfaces and reduces the complexity of the stress profile to a few membrane parameters that can be measured experimentally. For the case of asymmetric adsorption, we introduce a simulation protocol based on two bilayers separated by two aqueous compartments with different adsorbate concentrations. The adsorption of small particles with a size below 1 nm is shown to generate large spontaneous curvatures up to about 1/(24 nm). Our computational approach is quite general: it can be applied to any molecular model of bilayer membranes and can be extended to other mechanisms for the generation of spontaneous curvatures as provided, e.g., by asymmetric lipid composition or depletion layers of solute molecules. © *2015 Author(s). All article content, except where otherwise noted, is licensed under a Creative Commons Attribution 3.0 Unported License.* [http://dx.doi.org/10.1063/1.4906149]

I. INTRODUCTION

The basic building blocks of both biological and biomimetic membranes are lipid bilayers consisting of two lipid monolayers or leaflets.[1] Biological membranes are asymmetric in the sense that their two leaflets differ in their lipid composition.[2] This bilayer asymmetry has been recently mimicked in synthetic lipid bilayers produced by different preparation methods.[3,4] In addition, the two sides of the bilayer membranes are typically exposed to aqueous solutions that differ in their ionic or molecular composition. Any asymmetry between the two leaflets should induce a preferred or spontaneous curvature in the bilayer membranes which then try to adapt their shape to this curvature. One mechanism for the generation of spontaneous curvature is provided by asymmetric adsorption onto the two surfaces of the bilayer membranes. The latter mechanism has been theoretically predicted some time ago[5] but it has been realized only recently that the same mechanism should be responsible for the morphological transformations of membranes as frequently observed during protein adsorption onto vesicles or liposomes.[6]

Indeed, the adsorption of proteins onto liposomes often leads to dramatic changes in the liposome morphologies via the formation of membrane nanotubes or tubules. Examples are provided by N-BAR proteins such as amphiphysin[7,8] and endophilin,[9] F-BAR proteins such as syndapins,[10] and other proteins involved in endocytosis such as epsin.[11] In the experimental studies of these adsorption processes, the liposomes have not been characterized in detail but were typically multilamellar. More recently, two different *unilamellar* systems have also been found to undergo tubulation in the absence of external mechanical forces. One of these systems is provided by supported lipid bilayers that were exposed to a variety of antimicrobial peptides.[12–15] The other system consists of giant vesicles in contact with aqueous solutions of polyethylene glycol (PEG) and dextran.[16]

In the latter two systems, the tubules were quite stable over extended periods of time, which implies that they were stabilized by constant spontaneous curvatures.[6,16] This curvature describes the intuitive notion that thin layers with two chemically different sides tend to bend or bulge towards one of these sides. This bending or curvature preference was first described by Bancroft for surfactant monolayers in water-oil emulsions[17,18] and was included by Frank, as the so-called "splay term," in his theory for the curvature elasticity of liquid crystals.[19] In the context of lipid bilayers, spontaneous curvature was first considered by Helfrich,[20] in analogy to the liquid crystal case.

The Bancroft view of spontaneous curvature is based on the idea that a thin fluid layer is bounded by two interfaces

a)Electronic mail: lipowsky@mpikg.mpg.de

 © Author(s) 2015

This article is copyrighted as indicated in the article. Reuse of AIP content is subject to the terms at: http://scitation.aip.org/termsconditions. Downloaded to IP: 141.14.232.254 On: Tue, 03 Feb 2015 17:28:05

and that these interfaces typically differ in their tensions. Such a layer should have a tendency to bend or bulge towards the interface with the lower tension, because the layer can then reduce the area of the other interface with the higher tension. Based on this intuitive picture, one can develop an analytical theory for the preferred or spontaneous curvature of bilayer membranes when their two leaflets are exposed to different concentrations of adsorbing particles.[5,6] The defining property of these particles is that they do not permeate the membranes on experimentally relevant time scales. Thus, the particles may represent a variety of chemical species such as ions, small molecules, or peptides. One surprising prediction of the analytical theory is that the asymmetric adsorption of even fairly small particles such as ions may induce large spontaneous curvatures of the order of 1/(20 nm). So far, this prediction has not been scrutinized by systematic experiments or simulations.

In this paper, we study the spontaneous curvature of bilayer membranes by computer simulations. We use coarse-grained molecular dynamics simulations to study generic properties of the membrane systems[21–24] but our computational approach is general and can be easily applied to any molecular model of the membranes. We first calculate the stress or pressure profile across the bilayer from which we determine the mechanical tension within the membrane. In their natural reference states, the membranes are tensionless in the sense that they experience (almost) no mechanical tension.[21] Tensionless states of symmetric bilayers can be used to determine the bending rigidity from the undulation spectrum[25–28] and the Gaussian curvature modulus from the stress profile.[29,30] Here, we will study tensionless states of asymmetric bilayers and expand their properties around symmetric and tensionless reference states.

The spontaneous curvature of the bilayer membranes is determined using two computational approaches. On the one hand, we calculate the spontaneous curvature from the first moment of the stress profile.[31–33] This method relies on the detailed structure of the stress profile which is quite complex and can hardly be measured experimentally. On the other hand, we start from the intuitive view of spontaneous curvature arising from different tensions of the two leaflet-water interfaces. We reconsider these tensions and define them in terms of the mechanical tensions acting within the two leaflets of the bilayer membrane. In this way, we clarify some conceptual issues related to membrane tension and, at the same time, focus on quantities that can be easily obtained from the simulations.

We apply our computational approaches to two different types of asymmetric bilayers as depicted in Fig. 1. First, we consider bilayers that have a different lipid density within their two leaflets, see Fig. 1(a). For the flat state of such a bilayer as shown in the left cartoon of Fig. 1(a), the denser leaflet is compressed whereas the other leaflet is stretched. Thus, both leaflets can reduce their free energy if the bilayer bends or bulges towards the denser leaflet as in Fig. 1(a). Second, we study bilayers that have a different density of adsorbed particles at or within their two head group layers, see Fig. 1(b). In this case, the adsorbate particles increase the pressure in the two-dimensional head group layer, thereby reducing the mechanical tension in this layer. Because this reduction increases with increasing adsorbate density, the bilayer bulges towards the leaflet with the denser adsorbate layer as previously derived[5,6] from the Gibbs adsorption equation.

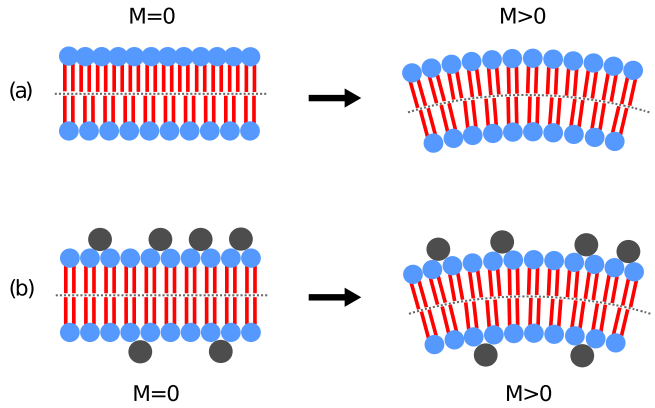

FIG. 1. Two molecular mechanisms for bilayer asymmetry: (a) Different lipid densities within the two leaflets and (b) different adsorbate densities at or within the two head group layers. The lipid head groups are shown in blue, the lipid tails in red, and the adsorbate "particles" in dark gray; the mean curvature of the membrane patches is denoted by M. In the left cartoon of (a), the upper leaflet has a higher lipid density and, thus, experiences a lower mechanical tension than the lower leaflet. In the left cartoon of (b), the upper head group layer has a higher density of adsorbate particles which then exert a higher pressure onto the head groups. In both cases, the bilayer should have a tendency to bulge towards the upper leaflet as in the right cartoons of (a) and (b), corresponding to positive mean curvature $M > 0$.

The results of our simulations fully corroborate the predictions of the analytical theory and show explicitly that relatively large spontaneous curvatures can be induced by the adsorption of relatively small particles. In fact, we find that the absolute value of the spontaneous curvature grows up to 1/(24 nm) when we increase the difference between the particle concentrations within the two aqueous compartments up to 320 mM. In addition, our simulations also demonstrate that the Gibbs adsorption equation does, in fact, apply to the mechanical tensions within the bilayer leaflets as considered here. The latter result is rather interesting from a conceptual point of view.

As previously discussed in Refs. 34 and 35, the concept of membrane tension is somewhat delicate and can easily lead to confusion. In particular, it is important to note that the tension of a membrane must be distinguished from the tension of an interface between two liquid phases. In the latter case, the tension can be derived both from a mechanical and from a thermodynamic point of view. In contrast, when we consider a membrane, we can still define its mechanical tension via the membrane's stress profile but the thermodynamic tension does not represent a meaningful concept because the membrane can reorganize and adapt different morphologies in the thermodynamic limit of large membrane area. Indeed, in the latter limit, tense membranes rupture whereas tensionless or compressed membranes crumple. Nevertheless, as shown by our present study, the Gibbs adsorption equation, which follows from the *thermodynamics* of liquid-liquid interfaces, can also be applied to the adsorption onto the two leaflet-water interfaces bounding the bilayer membrane if we identify the tension of such an interface with the *mechanical* tension within the corresponding bilayer leaflet.

Our paper is organized as follows. In Sec. II, we first emphasize that membrane curvature should be regarded as

This article is copyrighted as indicated in the article. Reuse of AIP content is subject to the terms at: http://scitation.aip.org/termsconditions. Downloaded to IP: 141.14.232.254 On: Tue, 03 Feb 2015 17:28:05

a collective property of many lipid molecules, describe our simulation setup, and study the elastic properties of symmetric bilayers, which provide a useful reference system with vanishing spontaneous curvature. In Sec. III, we introduce a general computational method to determine the spontaneous curvature from a few parameters that characterize the two leaflets of the bilayer membrane. A finite spontaneous curvature is induced in Sec. IV by preparing bilayers with two leaflets that differ in their lipid density. In Sec. V, we study the spontaneous curvature arising from the asymmetric adsorption of particles. In both cases, the spontaneous curvature can be understood and quantitatively described via the leaflet parameters. At the end, we give a brief outlook on the generality of our approach and on its applicability to other mechanisms for the generation of spontaneous curvature.

II. COMPUTATIONAL APPROACH

A. Membrane curvature as a collective property

Curvature is a geometric concept, originally developed by mathematicians to characterize the shape of smooth surfaces. Membranes appear to be rather smooth when viewed in the optical microscope but this smoothness does *not* persist to molecular scales. Indeed, because membranes are immersed in liquid water, each lipid and protein molecule within the membrane undergoes Brownian motion, which involves displacements both parallel and perpendicular to the membrane. The perpendicular displacements represent molecular protrusions that roughen the two interfaces bounding the membrane, see Fig. 2.

Therefore, in order to characterize a lipid/protein bilayer by its curvature, one has to consider small membrane patches and average over the molecular conformations within these patches. The minimal lateral size of these patches can be determined from the analysis of molecular dynamics simulations and was found to be about 1.5 times the membrane thickness, see Ref. 25 and Fig. 2. For a lipid bilayer with a thickness of 4 nm, this minimal size is about 6 nm.

A lipid bilayer patch with a lateral size of 6 nm contains about 80 to 100 lipid molecules. Therefore, membrane curvature should be viewed as a supramolecular feature arising from the collective behavior of a large number of lipid molecules. The same conclusion applies to the *spontaneous* curvature of membranes as studied in Secs. III–V.

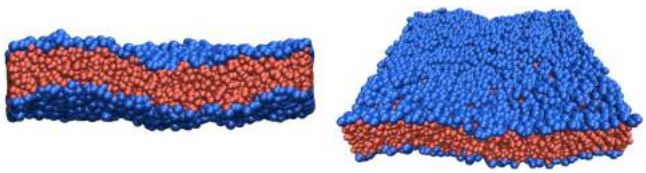

FIG. 2. Typical conformation of a lipid bilayer as observed in our simulations. The bilayer has a thickness of about 5 bead diameters and is bounded by two interfaces that are roughened by molecular protrusions, which displace the head groups (blue beads) perpendicular to the membrane. In order to characterize such a membrane by its curvature, one has to average over membrane segments with a lateral size that exceeds about 1.5 times the bilayer thickness, as follows from the spectral analysis of the membrane's shape fluctuations, see further below.

B. Dissipative particle dynamics (DPD)

DPD is a coarse-grained molecular dynamics technique with explicit solvent and local momentum conservation. The DPD particles, or "beads," represent either a number of identical molecules or several molecular groups, rather than single atoms. The internal degrees of freedom of these molecules or molecular groups are reflected by dissipative forces and random forces. The chemical nature of the molecules and molecular groups—for example, their hydrophobicity and hydrophilicity—is taken into account by conservative forces. Because all forces conserve momentum, DPD reproduces the correct hydrodynamics.

1. Basic simulation parameters

Our coarse-grained model includes water, lipid molecules, and adsorbate particles. Small water volumes are represented by single W beads, the adsorbate particles by single P beads. A lipid molecule consists of three hydrophilic H beads and two hydrophobic chains, each consisting of six C beads, which extends the chains used in Refs. 21 and 34 by two beads.

All beads have the same diameter d and the same mass $m_{\rm be}$, and these two quantities provide the basic length and mass units. In order to obtain a complete set of mechanical units, we also choose the thermal energy $k_{\rm B}T$ to be the basic energy unit, where $k_{\rm B}$ is the Boltzmann constant and T the absolute temperature. As a consequence, the basic time scale is given by $\tau = \sqrt{d^2\, m_{\rm be}/k_{\rm B}T}$. Furthermore, in the simulations described here, the equations of motion were discretized with the time step $\Delta t = 0.01\,\tau$.

The standard DPD parametrization of water corresponds to the bulk density $\rho = 3/d^3$, which matches the water compressibility at room temperature $T = 298$ K.[36] This choice for the molar density of water implies the mass density $3m_{\rm be}/d^3$ and determines the ratio $m_{\rm be}/d^3$ in physical units. In order to determine the length and time scales d and τ in physical units as well, one has to study certain system properties in the simulations and compare their values as obtained in units of d and τ with the experimentally measured values. For a lipid bilayer, two such properties are provided by the molecular area per lipid and the lateral diffusion constant of the lipids within the bilayer as described in Ref. 34. As a result, one obtains that the bead diameter d is of the order of 1 nm and the basic time scale τ is of the order of 1 ns. In the following, we will use a certain definition of the membrane thickness in order to obtain the specific value $d \simeq 0.8$ nm.

2. Forces acting on the beads

The DPD force that a bead j exerts on a bead i is the sum of three pairwise-additive forces: (i) the conservative force $\vec{F}_{ij}^{\,C}$, which arises from bonded and nonbonded interactions of the beads; (ii) the dissipative or viscous friction force $\vec{F}_{ij}^{\,D}$; and (iii) the random force $\vec{F}_{ij}^{\,R}$. The dissipative force is related to the relative velocity $\vec{v}_{ij} = \vec{v}_i - \vec{v}_j$ of the beads via

$$\begin{aligned} \vec{F}_{ij}^{\,D} &= -\gamma_{ij}\big(1 - r_{ij}/d\big)^2\big(\hat{r}_{ij}\cdot\vec{v}_{ij}\big)\hat{r}_{ij} \qquad \text{for} \quad r_{ij} < d \\ &= 0 \qquad\qquad\qquad\qquad\qquad\qquad\quad \text{for} \quad r_{ij} > d \end{aligned} \tag{1}$$

This article is copyrighted as indicated in the article. Reuse of AIP content is subject to the terms at: http://scitation.aip.org/termsconditions. Downloaded to IP: 141.14.232.254 On: Tue, 03 Feb 2015 17:28:05

with friction coefficients $\gamma_{ij} = \gamma_{ji}$ that depend on the bead type, the distance $r_{ij} = |\vec{r}_i - \vec{r}_j|$ between beads i and j, the unit vector $\hat{r}_{ij} = (\vec{r}_i - \vec{r}_j)/r_{ij}$ pointing from bead j to bead i, and the bead diameter d.

The random force $\vec{F}^R_{ij}$ represents thermal noise and has the form

$$\begin{aligned} \vec{F}^R_{ij} &= \sqrt{2\gamma_{ij}k_BT}\,(1 - r_{ij}/d)\,\zeta_{ij}\hat{r}_{ij} \qquad \text{for} \quad r_{ij} < d \\ &= 0 \qquad\qquad\qquad\qquad\qquad\qquad\quad \text{for} \quad r_{ij} > d \end{aligned} \tag{2}$$

with random forces ζ_{ij}. The latter forces are taken to correspond to Gaussian white noise with average value $\langle \zeta_{ij}(t) \rangle = 0$ and correlation function $\langle \zeta_{ij}(t)\zeta_{i'j'}(t') \rangle = \delta_{ii'}\delta_{jj'}\delta(t - t')$.

Adjacent beads in lipid molecules are connected by virtual springs using harmonic potentials

$$V_{\text{bond}}(r) = \tfrac{1}{2}\, k_r (r - r_{\text{eq}})^2 \tag{3}$$

for the separation r between two adjacent beads with the spring constant $k_r = 128\, k_BT/d^2$ and the equilibrium separation $r_{\text{eq}} = d/2$. The two hydrophobic chains of the lipid molecules are stiffened by the bending potential[21]

$$V_{\text{bend}}(\theta) = k_\phi \left[1 - \cos(\theta - \theta_{\text{eq}})\right] \tag{4}$$

that acts between two consecutive bonds along each chain. The bending constant is $k_\phi = 15\, k_BT$, and the tilt angle θ between two neighboring bonds attains the equilibrium value $\theta_{\text{eq}} = 0$ for collinear bonds.

In addition to the forces arising from the bonded interactions as specified above, all pairs of DPD beads exhibit the soft repulsive forces

$$\begin{aligned} \vec{F}^C_{ij} &= a_{ij}(1 - r_{ij}/d)\hat{r}_{ij}, \qquad \text{for} \quad r_{ij} < d \\ &= 0 \qquad\qquad\qquad\quad \text{for} \quad r_{ij} > d \end{aligned}, \tag{5}$$

with a repulsion strength a_{ij} that depends on the types of the two beads i and j, see Table I. The different repulsion strengths reflect the chemical nature of the beads, i.e., their hydrophobicity or hydrophilicity.

To simulate adsorption of small molecules onto membranes, we choose the DPD interaction parameters a_{ij} in such a way that the adsorbate beads partition between the water and the head group layers, see Table I. To prevent lipid flip-flops, i.e., the exchange of lipids between the two leaflets and to sustain the initial bilayer asymmetry, we have modified the lipid model introduced in Ref. 34 as follows. First, we increased the head-tail interaction parameter a_{HC} from $35\, k_BT/d$ to $50\, k_BT/d$, see Table I. Second, we increased the chain length from 4 to 6 chain beads per lipid tail. We have checked that, using this parameter set, lipid flip-flops were suppressed in asymmetric bilayers over microsecond time scales.

TABLE I. DPD interaction parameters a_{ij} given in units of k_BT/d. Here, H, C, W, and P denote the lipid head beads, the lipid chain beads, the water beads, and the adsorbate particles, respectively.

a_{ij}	H	C	W	P
H	30	50	30	25
C	50	10	75	75
W	30	75	25	35
P	25	75	35	25

C. Reference system provided by symmetric bilayers

We performed DPD simulations in the NVT ensemble. To suppress finite size effects,[37] we chose the overall density of DPD beads in such a way that the water density away from the bilayer is equal to the bulk water density $\rho = 3/d^3$, see Fig. 3(a), corresponding to standard DPD conditions for the water beads.[36,37] This choice of the bulk water density implies the bulk pressure $P = 20.7\, k_BT/d^3$ arising from the interaction energy alone, i.e., without the constant contribution $\rho\, kBT = 3k_BT/d^3$ from the kinetic energy. We set the lateral size of the simulation box equal to $L_x = L_y = 32\, d$ and varied the box height L_z between $32\, d$ and $48\, d$.

We then studied single bilayer membranes spanning these simulation boxes and measured the density profiles of the water (W), lipid head (H), and lipid chain (C) beads. Examples for these profiles are shown in Fig. 3(a) for a symmetric and tensionless bilayer. The hydrophobic core of the bilayer is characterized by a large maximum in the C density profile. The position of this maximum defines both the midplane of the bilayer and the origin of the z-coordinate perpendicular to it. The H density profile has two smaller peaks which represent the two leaflet-water interfaces.

1. Stress profiles and mechanical tension

The mechanical tension Σ_{mec} within the bilayer was controlled by varying the number of lipid molecules and, thus, the projected area per lipid, A, for fixed base area $L_xL_y = (32\, d)^2$ of the simulation box. We were particularly interested

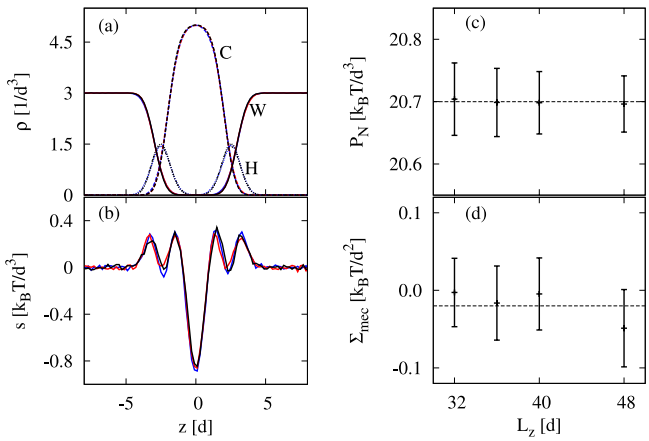

FIG. 3. Simulation results for symmetric and tensionless bilayers with projected lipid area $A = A_0 = 1.218\, d^2$: (a) Density profiles ρ as a function of the coordinate z perpendicular to the bilayer for water (W), lipid head (H), and lipid chain (C) beads. For large values of z, the water density ρ_W attains the value $\rho = 3/d^3$ corresponding to standard DPD conditions;[36] (b) the corresponding stress profile $s(z)$. The blue, red, and black lines correspond to box height $L_z = 32\, d$, $L_z = 40\, d$, and $L_z = 48\, d$, respectively; (c) the normal pressure component P_N is equal to the bulk pressure and has the constant value $P_N = 20.7\, kBT/d^3$, corresponding to the water density $\rho = 3/d^3$, for all values of the box height L_z; and (d) mechanical membrane tension Σ_{mec} as a function of the box height L_z which leads to the average value $\Sigma_{\text{mec}} = (-0.02 \pm 0.06)\, k_BT/d^2$ (dashed horizontal line), corresponding to a slight compression of the bilayer.

This article is copyrighted as indicated in the article. Reuse of AIP content is subject to the terms at: http://scitation.aip.org/termsconditions. Downloaded to IP: 141.14.232.254 On: Tue, 03 Feb 2015 17:28:05

in tensionless membranes for which $\Sigma_{\rm mec} \simeq 0$. In order to calculate the value of $\Sigma_{\rm mec}$, we computed the stress profiles

$$s(z) \equiv \Sigma_{\rm T}(z) - \Sigma_{\rm N} = -[P_{\rm T}(z) - P_{\rm N}] \tag{6}$$

as described previously in Refs. 21 and 34. The two quantities $P_{\rm T}$ and $P_{\rm N}$ are the diagonal elements of the pressure tensor P_{ij} with $P_{\rm T} = P_{xx} = P_{yy}$ and $P_{\rm N} = P_{zz}$. Because a liquid material cannot sustain a shear deformation in mechanical equilibrium, all off-diagonal terms P_{ij} with $i \neq j$ must vanish. Furthermore, the symmetry of our simulation box, with periodic boundary conditions in the x- and y-directions parallel to the bilayer membrane, implies that the pressure components can only depend on the coordinate z perpendicular to the membrane. In general, all components of the divergence of the pressure tensor, which is a vector with the Cartesian components $\sum_j \partial P_{ij}/\partial x_j$, must vanish.[38] In the present situation, the latter requirement leads to $\partial P_{zz}/\partial z = 0$ which implies that $P_{zz} = P_{\rm N}$ does not depend on z and is constant throughout the simulation box.

In Fig. 3(b), we display stress profiles $s(z)$ for different values of the height L_z of the simulation box. Inspection of this figure shows that these stress profiles are essentially independent of L_z and, thus, do not display L_z-dependent finite size effects. Likewise, the normal pressure component $P_{\rm N}$ does not depend on L_z and has a constant value equal to the bulk pressure $P = 20.7\ k_{\rm B}T/d^3$, see Fig. 3(c), corresponding to the bulk water density $\rho = 3/d^3$ far away from the bilayer. Note that the normal pressure would become L_z-dependent if we chose the *average* bead density, including the lipid beads, to be equal to $3/d^3$ as in Ref. 37.

The overall form of the stress profiles in Fig. 3(b) is similar to those obtained in earlier MD[21] and DPD[22] simulations: The hydrocarbon tail region is characterized by a negative stress applied from the outside in order to balance the internal pressure of the hydrocarbon tails. In contrast, the head group region is characterized by a positive stress that has to be applied from the outside in order to compensate the tendency of the head groups to decrease their contact area with the water.

Inspection of the head group region in Fig. 3(b) shows that this region is characterized by a double-peak structure. This feature can be understood by comparing the stress profile with the density profiles in Fig. 3(a). The inner peak of the stress profile close to the hydrophobic core of the bilayer corresponds to the interface between the lipid chain (C) and lipid head (H) beads whereas the outer peak close to the aqueous phase reflects the interface between the H and water (W) beads. The stress minimum between the two peaks arises from the pressure between the H beads, which may be viewed as a 2-dimensional liquid. This double-peak structure of the stress profile within the head group region persists to asymmetric membranes as discussed further below.

The mechanical tension $\Sigma_{\rm mec}$ of the membrane is obtained from the integral

$$\Sigma_{\rm mec} = \int_{-\infty}^{+\infty} {\rm d}z\ s(z) \simeq \int_{-L_z/2}^{+L_z/2} {\rm d}z\ s(z), \tag{7}$$

i.e., from the zeroth moment of the stress profile. As shown in Fig. 3(d), this quantity is found to be independent of the box height L_z, within the statistical error.

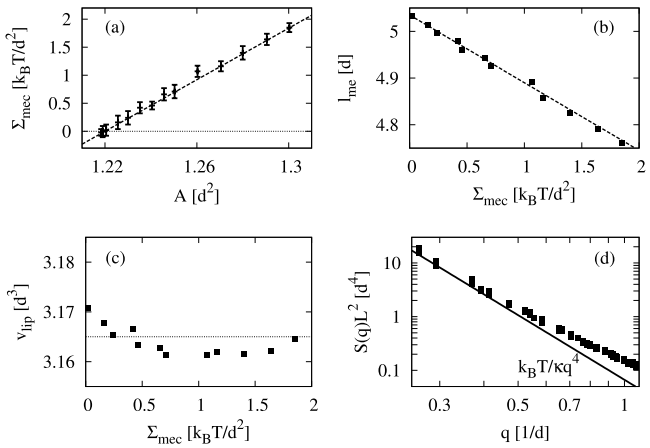

FIG. 4. Mechanical properties of symmetric bilayer membranes: (a) The mechanical tension $\Sigma_{\rm mec}$ of the membrane increases linearly with the projected area per lipid, A; (b) the membrane thickness $\ell_{\rm me}$ decreases linearly with the membrane tension $\Sigma_{\rm mec}$; (c) the average volume per lipid, $V_{\rm lip}$, remains essentially constant as the tension $\Sigma_{\rm mec}$ is changed; and (d) fluctuation spectrum S as a function of the wavenumber q for the tensionless state. The solid line represents Eq. (12) with $\kappa = 15\ k_{\rm B}T$ and provides a good fit to the simulation data (squares) for small values of q. This line describes the long-wavelength behavior of the spectrum S as described by $\sim k_{\rm B}T/(\kappa q^4)$ for a tensionless membrane.

The mechanical properties displayed in Fig. 4 correspond to an essentially tensionless membrane with tension $\Sigma_{\rm mec} = (-0.02 \pm 0.06)\ k_{\rm B}T/d^2$. The dependence of the membrane tension $\Sigma_{\rm mec}$ on the projected area per lipid, A, is displayed in Fig. 4(a). As shown in this figure, the membrane tension $\Sigma_{\rm mec}$ increases linearly with the projected area per lipid, A, whereas the membrane thickness $\ell_{\rm me}$ decreases linearly with the tension $\Sigma_{\rm mec}$, see Fig. 4(b). While both the projected lipid area A and the membrane thickness $\ell_{\rm me}$ vary with the membrane tension $\Sigma_{\rm mec}$, the average volume per lipid, $V_{\rm lip}$, is found to be essentially independent of $\Sigma_{\rm mec}$, see Fig. 4(c), in agreement with experimental results on the large volume compressibility modulus of lipid bilayers.[39]

2. Possible definitions of membrane thickness

The thickness displayed in Fig. 4(b) was determined by the following "grid method." The base area was partitioned into a square lattice with 16×16 equally sized squares. For each square, we determined the average values, $Z_1 > 0$ and $Z_2 < 0$, of the terminal head beads in the upper and lower leaflet of the bilayer, respectively. The local membrane thickness was then obtained by averaging $|Z_1| + |Z_2|$ over all squares of the lattice. The resulting thickness is equal to the distance between the two peaks of the density profile for the head groups.

The mechanical tension $\Sigma_{\rm mec}$ of the symmetric bilayer membrane vanishes at a certain projected lipid area $A = A_0$. For the DPD parameters in Table I, we obtained $A_0 \simeq 1.22\ d^2$ in our simulations. The corresponding membrane thickness $\ell_{\rm me}$ was found to be $\ell_{\rm me} = 5\ d$, as given by the distance between the two peaks of the head group density profile in Fig. 3(a).

The definition of the membrane thickness in terms of the head group densities is convenient in order to analyze the shape fluctuations of the bilayers. In general, the membrane thickness can be defined in a variety of ways using different density

This article is copyrighted as indicated in the article. Reuse of AIP content is subject to the terms at: http://scitation.aip.org/termsconditions. Downloaded to IP: 141.14.232.254 On: Tue, 03 Feb 2015 17:28:05

profiles. Thus, instead of the head group density profile, we may consider the water density profile and determine the z-coordinates $z = \ell_1 > 0$ and $z = \ell_2 < 0$ for which the local water density is equal to half its bulk value, i.e., for which $\rho_W(z_i) = \frac{1}{2}\rho = 3/(2d^3)$. The W density profile in Fig. 3(a) then leads to the membrane thickness $\ell_{me} \equiv (\ell_1 - \ell_2) = 6\ d$, which is somewhat larger than the value 5 d based on the head group density profile. On the other hand, we could also define the membrane thickness via its hydrophobic core as provided by the z-range for which the lipid chain density exceeds half its peak value at $z = 0$. Using the latter definition, we obtain the membrane thickness $\ell_{me} = 4\ d$ as follows from the C density profile in Fig. 3(a).

The membrane thickness can be used to determine the bead size d in physical units. For real lipid bilayers, the separation of the two head group layers is about 4 nm which implies that the bead diameter $d \simeq 4\ \text{nm}/5 = 0.8\ \text{nm}$.

3. Compressibility modulus and bending rigidity

Based on the data in Fig. 4(a), we determine the area compressibility modulus K_A from the linear relation

$$\Sigma_{mec} \approx K_A \frac{A - A_0}{A_0} \tag{8}$$

which represents the leading order term in the area stretching parameter $(A - A_0)/A_0$. As a result, we obtained $K_A = 28\ k_BT/d^2$. Using the relationship[25]

$$\kappa = K_A \ell_{me}^2/48 \tag{9}$$

between the membrane bending rigidity κ and the area compressibility modulus K_A as well as the measured membrane thickness $\ell_{me} = 5\ d$, we obtain the value $\kappa \simeq 15\ k_BT$ for the bending rigidity.

To corroborate this result for the bending rigidity, we analyzed the thermally excited shape fluctuations or undulations of the bilayer membranes. First, we performed simulations of a tensionless membrane in a cubic box of size $L_x = L_y = L_z = 48\ d$, and computed the fluctuation spectrum $S(q) = \langle |h_q|^2 \rangle$ directly from the Fourier components h_q of the membrane displacement field $h(x,y)$. The fluctuation spectrum obtained in this way is shown in Fig. 4(d). Next, we compare these simulation data for $S(q)$ with the expression

$$S(q) = \frac{k_BT}{L^2(\Sigma_{flu} q^2 + \kappa q^4)} \tag{10}$$

with $L \equiv L_x = L_y$ which depends on the fluctuation tension Σ_{flu}. Numerical simulations provided some evidence that this latter tension may be slightly different from the mechanical tension Σ_{mec}[40–42] whereas symmetry arguments and simulations of 1 + 1-dimensional membranes (or worm-like chains) supported the equality $\Sigma_{flu} = \Sigma_{mec}$,[43,44] an equality that we assumed implicitly in our original study of the fluctuation spectrum.[25,35] We will not address this issue here but focus on the intermediate range

$$\sqrt{\Sigma_{mec}/\kappa} \ll q \ll 1/\ell_{me} \tag{11}$$

of q-values for which the fluctuation spectrum attains the simple form

$$S(q) \approx \frac{k_BT}{L^2\,\kappa q^4} \tag{12}$$

even if the fluctuation tension Σ_{flu} were somewhat different from the mechanical tension Σ_{mec}. When we compare the simple expression (12) with the low q-range of our simulation data, we obtain good agreement provided we choose the value $\kappa = 15\ k_BT$ for the bending rigidity, see Fig. 4. This value agrees with the estimate for the bending rigidity as obtained above using the relation (9). For wave vectors that are comparable to or larger than $q_{max} = 2\pi/\ell_{me}$, the fluctuation spectrum reflects the small-scale roughness of the bilayer/water interfaces[25–28,45,46] arising from molecular protrusions as in Fig. 2.

III. BILAYER ASYMMETRY AND SPONTANEOUS CURVATURE

In this section, we discuss the related concepts of bilayer asymmetry and spontaneous curvature from a general point of view. As emphasized in Subsection II A, the spontaneous curvature should be regarded as a nanoscopic, coarse-grained quantity that applies to length scales that exceed twice the membrane thickness. The stress profile, on the other hand, reflects the molecular architecture of the lipids, see, e.g., the double-peak structure in Fig. 3(b). In the following, we first review the formal relation between the spontaneous curvature and the first moment of the stress profile as proposed by Helfrich in Ref. 31. This relation generalizes concepts as developed in classical elasticity theory for solid bodies[47] to fluid layers and has been confirmed by mean field theories for surfactant bilayers.[32,33] In addition, we reconsider the theoretical approach described in Refs. 5 and 6 based on the Bancroft view of spontaneous curvature,[17,18] in which the bilayer membrane is regarded as a thin fluid layer bounded by two leaflet-water interfaces. The tensions of the upper-leaflet-water and the lower-leaflet-water interfaces are now identified with the mechanical tensions, Σ_1 and Σ_2, within the corresponding leaflets. If the bilayer is asymmetric with $\Sigma_1 \neq \Sigma_2$, the corresponding interfacial free energy can be decreased by bending but this decrease is balanced by an increase in the membrane's bending energy. This free energy balance can be obtained by expanding the interfacial free energy of the leaflet-water interfaces and the bending energy of the neutral surface to first order in the mean curvature M. In this way, we obtain a simple and explicit expression for the spontaneous curvature m in terms of the tensions Σ_1 and Σ_2, the bending rigidity κ, and the thicknesses ℓ_1 and ℓ_2 of the two leaflets of the bilayer. Finally, we show that this expression becomes even simpler when we consider the case of small asymmetries and expand the leaflet parameters around the symmetric and tensionless bilayer state.

A. Spontaneous curvature from stress profile

First, we review the relation between the spontaneous curvature m and the first moment of the stress profile $s(z)$ as proposed in Ref. 31. This relation is based on several assumptions. First, in analogy to the bending of solid beams and plates, the microscopic torque (or bending moment) acting onto a

This article is copyrighted as indicated in the article. Reuse of AIP content is subject to the terms at: http://scitation.aip.org/termsconditions. Downloaded to IP: 141.14.232.254 On: Tue, 03 Feb 2015 17:28:05

cross-section of a planar bilayer is taken to be

$$\mathcal{T}_{\rm mic} = \int_{-\infty}^{+\infty} {\rm d}z\, s(z)\, z, \tag{13}$$

where pure bending implies no stretching and, thus, a tensionless membrane with $\Sigma_{\rm mec} = \int {\rm d}z\, s(z) = 0$. This relation embodies the usual assumption of classical elasticity theory that the stresses within an elastic body can be defined with respect to the coordinates of the undeformed body.[47] Second, one can also derive a nanoscopic torque based on the spontaneous curvature model for the shape of the membrane. Within this model, the bending energy of the membrane has the form[20,48]

$$\mathcal{E}_{\rm be} = \int d\mathcal{A}\, 2\kappa\,(M-m)^2 = \int d\mathcal{A}\, \frac{\kappa}{2}\,(C_1+C_2-2m)^2 \tag{14}$$

with the membrane area $\mathcal{A}$ and the mean curvature $M = \frac{1}{2}\,(C_1 + C_2)$, which represents the arithmetic mean of the two principal curvatures C_1 and C_2. The form of the nanoscopic torque depends on the choice of the coordinate system and becomes particularly transparent if one uses a tangent, principal frame.[49] For the special case of a minimal surface with vanishing mean curvature, the nanoscopic torque $\mathcal{T}_{\rm nan}$ is then found to be[31,49]

$$\mathcal{T}_{\rm nan} = \frac{\partial}{\partial C_i} 2\kappa (M-m)^2\Big|_{M=0} = -2\kappa m. \tag{15}$$

This relation for $M = 0$ applies, in particular, to a flat membrane. If we identify the nanoscopic and the microscopic torque and set $\mathcal{T}_{\rm nan} = \mathcal{T}_{\rm mic}$, we obtain the simple relation[31]

$$-2\kappa m = \int_{-\infty}^{+\infty} {\rm d}z\, s(z)\, z \tag{16}$$

between the spontaneous curvature m and the first moment of the stress profile. The same relation has also been obtained in Refs. 32 and 33 starting from local density functionals for surfactant bilayers. The approach in Ref. 32 used an expansion of the free energy around the planar state of the bilayer and showed explicitly, in the context of a mean field theory, that the relation as given by Eq. (16) involves the stress profile of the planar bilayer.

B. Spontaneous curvature from leaflet parameters

Now, we consider a large membrane segment and view it as a thin fluid layer, which is bounded by two membrane-water interfaces. In the planar state of the asymmetric bilayer, the upper leaflet has thickness ℓ_1 and interfacial area $\mathcal{A}_1 = \mathcal{A}$ while the lower leaflet has thickness ℓ_2 and interfacial area $\mathcal{A}_2 = \mathcal{A}$, see Fig. 5. The interfacial areas $\mathcal{A}_1$ and $\mathcal{A}_2$ are related to the projected area A per lipid molecule by $\mathcal{A}_1 = N_1 A$ and $\mathcal{A}_2 = N_2 A$ where N_1 and N_2 are the number of lipid molecules within the upper and the lower leaflet, respectively.

We now bend this membrane segment into a cylindrical or spherical segment, taking into account that the average volume per lipid and, thus, the volume of each leaflet is conserved during bending. If we further assume that the contact surface between the two leaflets has the same area before and after bending, i.e., that this contact surface represents the neutral surface (or surface of inextension), we find that the leaflets

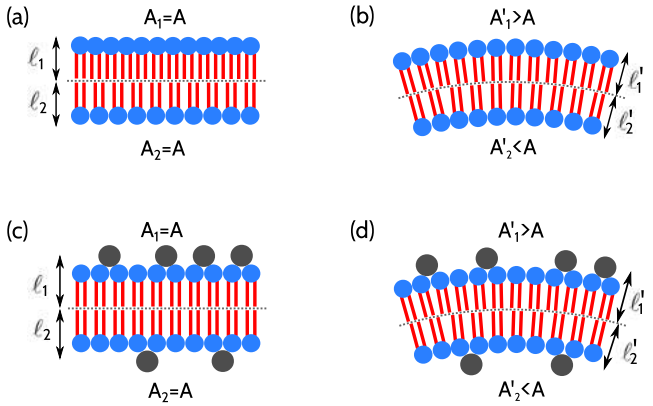

FIG. 5. Bilayer membranes with two leaflets that differ in their (a,b) lipid densities and (c,d) coverage by adsorbate particle (dark gray). In both cases, the geometry of the planar state in (a,c) is compared with the geometry of the curved state in (b,d). The simulations probe the planar state which is enforced by the periodic boundary conditions. In the latter state, the upper leaflet has thickness ℓ_1 and interfacial area $A_1 = A$ while the lower leaflet has thickness ℓ_2 and interfacial area $A_2 = A$. In the curved state, the upper leaflet has thickness ℓ'_1 and interfacial area $A'_1 > A$ while the lower leaflet has thickness ℓ'_2 and interfacial area $A'_2 < A$.

attain the thicknesses

$$\ell'_1 \approx \ell_1\,(1-\ell_1 M) \quad \text{and} \quad \ell'_2 \approx \ell_2\,(1+\ell_2 M) \tag{17}$$

up to first order in the mean curvature M of the membrane segment. In fact, when we expand the thicknesses ℓ'_1 and ℓ'_2 of the weakly curved leaflets in powers of the mean curvature M, dimensional analysis implies that

$$\ell'_1 \approx \ell_1\,(1+\alpha_1\ell_1 M) \quad \text{and} \quad \ell'_2 \approx \ell_2\,(1+\alpha_2\ell_2 M) \tag{18}$$

up to first order in M with dimensionless coefficients α_1 and α_2, irrespective of the precise position of the neutral surface.

The area of the upper-leaflet-water interface then behaves as

$$\mathcal{A}'_1 \approx \mathcal{A}(1+2\ell'_1 M) \approx \mathcal{A}(1+2\ell_1 M) \tag{19}$$

up to first order in M whereas the area of the lower-leaflet-water interface is asymptotically equal to

$$\mathcal{A}'_2 \approx \mathcal{A}(1-2\ell'_2 M) \approx \mathcal{A}(1-2\ell_2 M) \tag{20}$$

up to first order in M. Thus, to leading order in the mean curvature M, the interfacial areas $\mathcal{A}'_1$ and $\mathcal{A}'_2$ do not depend on the changes $\ell'_i - \ell_i$ of the interfacial thicknesses and, thus, do not depend on the precise position of the neutral surface.

We now assume, first in a somewhat heuristic manner, that we can characterize the two leaflet-water interfaces by two leaflet tensions, Σ_1 and Σ_2. As the bilayer is bent, the interfacial free energy is changed according to

$$\Delta\mathcal{F}_{\rm int} = \Sigma_1(\mathcal{A}'_1 - \mathcal{A}_1) + \Sigma_2(\mathcal{A}'_2 - \mathcal{A}_2) \tag{21}$$

which has the asymptotic behavior

$$\Delta\mathcal{F}_{\rm int} \approx 2(\ell_1\,\Sigma_1 - \ell_2\,\Sigma_2)\, M\,\mathcal{A} \tag{22}$$

up to first order in M.

We now want to relate this change in the interfacial free energy of the two leaflets to the bending energy of the neutral surface. In the spontaneous curvature model as given by Eq. (14),

This article is copyrighted as indicated in the article. Reuse of AIP content is subject to the terms at: http://scitation.aip.org/termsconditions. Downloaded to IP: 141.14.232.254 On: Tue, 03 Feb 2015 17:28:05

the bending energy of the neutral surface is given by

$$\mathcal{E}_{\rm be} = 2\kappa(M-m)^2\mathcal{A} \approx (2\kappa m^2 - 4\kappa m M)\mathcal{A} \tag{23}$$

up to first order in M which depends on the bending rigidity κ and the spontaneous curvature m. If we identify the terms of order M in Eqs. (22) and (23) or use the equivalent relation

$$\left.\frac{\partial \mathcal{E}_{\rm be}}{\partial M}\right|_{M=0} = \left.\frac{\partial \Delta\mathcal{F}_{\rm int}}{\partial M}\right|_{M=0}, \tag{24}$$

we obtain the identity

$$2\kappa m = \Sigma_2\,\ell_2 - \Sigma_1\,\ell_1 \tag{25}$$

which expresses the product $2\kappa m$ in terms of four leaflet parameters, namely, the two leaflet thicknesses ℓ_1 and ℓ_2 as well as the two leaflet tensions Σ_1 and Σ_2.

C. Leaflet tensions and thicknesses

In order to define the tensions of the two leaflet-water interfaces, one could decompose the stress profile, as displayed in Fig. 3(b) for a symmetric bilayer, into a hydrophobic core region and two head group layers. However, this decomposition is not unique and requires the introduction of somewhat arbitrary boundaries between the hydrophobic core and the head group layers. We therefore did not utilize such a decomposition into three distinct layers. Instead, we made use of the fact that all simulations, both for the symmetric and for the asymmetric bilayers, led to a pronounced maximum for the density profile of the C beads and defined the midplane of the bilayer membrane by the position of this maximum. Here and below, we choose the z-coordinate in such a way that this midplane is located at $z = 0$. This midplane is then used to decompose the stress profile for the whole bilayer into two stress profiles for the two leaflets. Using this decomposition, we define the leaflet tensions Σ_1 and Σ_2 by

$$\Sigma_1 \equiv \int_0^{L_z/2} {\rm d}z\, s(z) \quad \text{and} \quad \Sigma_2 \equiv \int_{-L_z/2}^{0} {\rm d}z\, s(z), \tag{26}$$

i.e., by integrating the stress profile $s(z)$ over each leaflet separately. These tensions do not involve any additional parameter and lead to the simple decomposition

$$\Sigma_{\rm mec} = \int_{-L_z/2}^{L_z/2} {\rm d}z\, s(z) = \Sigma_1 + \Sigma_2 \tag{27}$$

of the mechanical tension $\Sigma_{\rm mec}$ as given by Eq. (7). Note that a positive mechanical tension leads to a stretched bilayer membrane whereas a negative mechanical tension leads to a compressed membrane. Likewise, positive values of the leaflet tension Σ_i imply that the corresponding leaflet is stretched whereas negative values of Σ_i correspond to a compression of this leaflet.

The calculation of the stress profile involves a relatively large computational effort and its precise z-dependence is difficult to calculate with high precision. The leaflet tensions Σ_1 and Σ_2 as given by Eq. (26) involve half-space integrals over the stress profile for which the noise in the data is smoothened out in a uniform manner. In contrast, the first moment of the stress profile, which determines the spontaneous curvature via Eq. (16), leads to an amplification of the noise within the head group region where the stress profile has a particularly complex structure. This computational advantage of Eq. (26) compared to Eq. (16) is further enhanced if we express the leaflet tensions Σ_1 and Σ_2 in terms of the coverages by adsorbate particles, see Sec. V below, because the coverages are obtained from density profiles which can be calculated with much higher precision.

The whole line of arguments used to derive the relation (25) for the spontaneous curvature did not depend on any specific definition of the leaflet thicknesses ℓ_1 and ℓ_2. In fact, using the leaflet tensions Σ_1 and Σ_2 as given by Eq. (26), we can define these thicknesses in such a way that the two relations (25) and (16) become identical. These definitions are provided by

$$\ell_1 \equiv \frac{\int_0^{L_z/2} dz\, s(z) z}{\int_0^{L_z/2} dz\, s(z)} = \frac{1}{\Sigma_1}\int_0^{L_z/2} dz\, s(z) z \tag{28}$$

and

$$\ell_2 \equiv \frac{\int_{-L_z/2}^{0} dz s(z)|z|}{\int_{-L_z/2}^{0} dz s(z)} = \frac{1}{\Sigma_2}\int_{-L_z/2}^{0} dz\, s(z)|z|. \tag{29}$$

D. Small asymmetries between the two leaflets

As emphasized in Sec. II A, large values of the spontaneous curvature m that exceed the value $1/(1.5\,\ell_{\rm me})$ are not physically meaningful because the membrane cannot attain a mean curvature of this size without severe distortions of its bilayer structure. It turns out that relatively small asymmetries already lead to unphysically large values of m. Therefore, it is sufficient to focus on small asymmetries and to expand the leaflet parameters for the asymmetric bilayers around their values for the symmetric case.

For a symmetric bilayer, the stress profile $s(z) = s_{\rm sy}(z)$ satisfies the symmetry relation $s_{\rm sy}(-z) = s_{\rm sy}(z)$ which implies

$$\Sigma_2 = \Sigma_1 = \tfrac{1}{2}\int_{-L_z/2}^{L_z/2} {\rm d}z\, s_{\rm sy}(z) = \tfrac{1}{2}\,\Sigma_{\rm mec} \equiv \Sigma_{\rm sy}. \tag{30}$$

Furthermore, for a symmetric *and tensionless* bilayer with stress profile $s(z) = s_{{\rm sy},0}(z)$, the relation (30) simplifies and becomes

$$\Sigma_{\rm sy} = \int_0^{L_z/2} {\rm d}z\, s_{{\rm sy},0}(z) = \int_{-L_z/2}^{0} {\rm d}z\, s_{{\rm sy},0}(z) = 0. \tag{31}$$

We now consider small asymmetries and write the leaflet thicknesses in the form

$$\ell_i = \ell_{\rm sy} + \delta\ell_i \quad \text{for} \quad i = 1, 2, \tag{32}$$

where $\ell_{\rm sy}$ is the thickness of one leaflet in the absence of the asymmetry. Likewise, the leaflet tensions are decomposed according to

$$\Sigma_i = \Sigma_{\rm sy} + \delta\Sigma_i \quad \text{for} \quad i = 1, 2, \tag{33}$$

where $\Sigma_{\rm sy}$ is the tension of both leaflets for the symmetric bilayer, as in Eqs. (30) and (31). Because the asymmetric bilayers considered here are taken to be tensionless as well, we also have $\Sigma_{\rm mec} = \Sigma_1 + \Sigma_2 = 0$ for these bilayers which implies

$$\delta\Sigma_2 = -\delta\Sigma_1 \quad \text{(asymmetric, tensionless)}. \tag{34}$$

This article is copyrighted as indicated in the article. Reuse of AIP content is subject to the terms at: http://scitation.aip.org/termsconditions. Downloaded to IP: 141.14.232.254 On: Tue, 03 Feb 2015 17:28:05

When we insert the expansions around the symmetric bilayer as given by Eqs. (32) and (33) into the right hand side of Eq. (25), we obtain

$$2\kappa m \approx \ell_{sy}(\delta\Sigma_2 - \delta\Sigma_1) + \Sigma_{sy}(\delta\ell_2 - \delta\ell_1) \tag{35}$$

to leading order in the deviations from the symmetric state. If we now take the reference state to be both symmetric *and tensionless*, the leaflet tension Σ_{sy} vanishes, see Eq. (31), and so does the second term on the right hand side of Eq. (35). As a result, we are then left with the simpler relation

$$2\kappa m \approx \ell_{sy}(\delta\Sigma_2 - \delta\Sigma_1) = -2\ell_{sy}\,\delta\Sigma_1 \tag{36}$$

between the product κm of bending rigidity and spontaneous curvature, the leaflet thickness ℓ_{sy} of the symmetric reference state, and the deviations $\delta\Sigma_1$ and $\delta\Sigma_2$ of the leaflet tensions from their values in the symmetric state where the identity $\delta\Sigma_2 = -\delta\Sigma_1$ for asymmetric and tensionless bilayers as in Eq. (34) has been used.

In Secs. IV–V, we will study the spontaneous curvatures as generated by asymmetric lipid densities and asymmetric adsorbate layers. We will then consider the term $2\ell_{sy}$ in Eq. (36) as an effective membrane thickness ℓ_{me}. The value of this thickness turns out to be close to what one would obtain from a naive estimate. Furthermore, in the case of asymmetric adsorption, we can replace the excess tension $\delta\Sigma_1$, which can hardly be measured experimentally, by the coverage of the adsorbate particles, which represents a measurable quantity, see Sec. V below.

IV. BILAYERS WITH ASYMMETRIC LIPID DENSITIES

A. Control parameter for density asymmetry

We now consider asymmetric bilayers with N_1 lipids in the upper leaflet and N_2 lipids in the lower leaflet, see Fig. 6. The associated bilayer asymmetry is characterized by the mole fraction

$$\phi \equiv N_1/(N_1 + N_2) \tag{37}$$

of the upper leaflet. For symmetric bilayers, one has $N_1 = N_2$, i.e., $\phi = 1/2$. Without loss of generality, we take $N_1 \geq N_2$ and thus consider membranes with mole fractions $\phi \geq 1/2$. The projected area per lipid is now defined as

$$A \equiv 2L_xL_y/(N_1 + N_2). \tag{38}$$

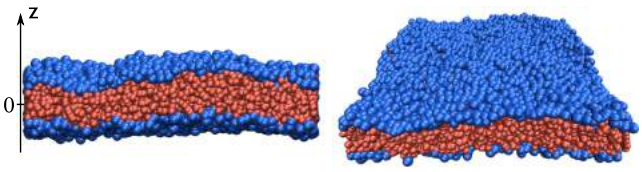

FIG. 6. Simulation snapshots (side and oblique view) of a bilayer membrane with asymmetric lipid densities. Lipid head groups are shown in blue and lipid chains in red. The water beads are not shown for clarity. The upper leaflet contains $N_1 = 920$ lipids, the lower leaflet $N_2 = 738$ lipids. As previously mentioned, the maximum of the lipid chain (C) density defines the midplane of the bilayer as well as the origin $z = 0$ of the z-coordinate perpendicular to it. The mean curvature is taken to be positive if the membrane bulges towards the upper leaflet, i.e., towards positive z-values.

We performed DPD simulations in the NVT ensemble at different mole fractions ϕ and lipid areas A. In our simulations, we used a simulation box with the base area $L_x \times L_y = 32\,d \times 32\,d$ and studied the three values $L_z = 32\,d$, $L_z = 40\,d$, and $L_z = 48\,d$ for the box height. In each case, we adjusted the overall density of the DPD beads in such a way that the water density away from the bilayer was equal to the bulk water density $\rho = 3/d^3$. The normal pressure P_N is then equal to the pressure of pure water at standard DPD conditions, which is given by $P = 20.7\,k_BT/d^3$ as mentioned before. The time of a single simulation was $2 \times 10^5\Delta t = 2 \times 10^3\tau$, which corresponds to about 2 μs because the basic time scale τ in the DPD simulations is of the order of 1 ns.[34]

We have checked that the lipid numbers N_1 and N_2 in the upper and lower leaflet remain constant throughout our simulation runs if the mole fractions ϕ satisfy the inequality $\phi < 0.58$. For membranes with larger initial asymmetry, $\phi > 0.58$, we could observe flip-flops of lipids from the upper to the lower leaflet, which leads to a reduction of the lipid fraction ϕ in the course of the simulations. Therefore, we only studied membranes with mole fractions $\phi < 0.58$ for which the membrane asymmetry remains unchanged during the simulation time of a few μs. One should note, however, that flip-flops are expected to occur for any value of ϕ on sufficiently long time scales. The limiting value $\phi = 1/2$ corresponds to an optimal packing of the lipids for which flip-flop times of the order of half an hour or longer have been observed experimentally. Therefore, the spontaneous curvatures that we compute here apply to time scales that are small compared to the typical flip-flop times. In this sense, we consider the constrained equilibrium of bilayers without flip-flops. For phospholipid bilayers with flip-flop times of the order of half an hour, this type of equilibrium is certainly accessible to experimental studies.

B. Spontaneous curvature from stress profile

We first increased the fraction ϕ by flipping groups of lipids from the lower to the upper leaflet. These flips were performed while keeping both the total number of lipid molecules, $N_1 + N_2$, and the lateral box dimensions, L_x and L_y, fixed. In this way, we increased the fraction ϕ for a constant value of the projected area per lipid, A, as defined in Eq. (38). The associated mechanical tensions are displayed in Fig. S1.[50] Inspection of this figure shows that such an increase of the fraction ϕ, for a given molecular area $A > A_0$, leads to a decrease of the mechanical membrane tension Σ_{mec}, until this tension vanishes at a certain threshold value $\phi = \phi_0$ of the lipid mole fraction in the upper leaflet. The computed values of ϕ_0 are given in Table II for different lipid areas A. Stress profiles of asymmetric and tensionless membranes with different mole fractions $\phi = \phi_0$, corresponding to different molecular areas A, are displayed in Figs. 7 and S2.[50] These stress profiles can be understood as follows. The increased density of lipids in the upper leaflet acts to decrease the mechanical tension Σ_1 within the upper leaflet. On the other hand, when we focus on the contribution of the head group region to Σ_1, the decrease of Σ_1 can be understood in terms of the increased density of the upper headgroup layer which provides a better shielding of the hydrophobic tails from the water. In contrast, the decreased

This article is copyrighted as indicated in the article. Reuse of AIP content is subject to the terms at: http://scitation.aip.org/termsconditions. Downloaded to IP: 141.14.232.254 On: Tue, 03 Feb 2015 17:28:05

TABLE II. Molecular area A, mole fraction ϕ_0, mechanical tension $\Sigma_{\rm mec}$, and the product $2\kappa m$ for asymmetric and tensionless bilayers. The product $2\kappa m$ was determined via Eq. (16) from the first moment of the stress profiles in Figs. 7 and S2.[50] The spontaneous curvature m in the last column was then calculated from $2\kappa m$ using the value $\kappa = 15\,k_BT$ for the bending stiffness. All quantities are given in units of the bead diameter d, which provides the basic length scale for our system, and of the basic energy scale k_BT.

$A\,(d^2)$	ϕ_0	$\Sigma_{\rm mec}\,(k_BT/d^2)$	$2\kappa m\,(k_BT/d)$	$m\,(1/d)$
1.221	0.514	0.004 ± 0.059	2.07 ± 0.64	0.069 ± 0.021
1.222	0.522	0.009 ± 0.074	3.41 ± 0.44	0.114 ± 0.015
1.225	0.532	0.020 ± 0.026	4.61 ± 0.35	0.154 ± 0.012
1.230	0.545	−0.004 ± 0.046	5.77 ± 0.18	0.192 ± 0.006
1.235	0.555	−0.004 ± 0.022	7.31 ± 0.38	0.244 ± 0.013
1.240	0.570	−0.004 ± 0.021	9.19 ± 0.68	0.306 ± 0.023
1.245	0.576	0.018 ± 0.032	9.90 ± 0.46	0.330 ± 0.015

density of lipids in the lower leaflet acts to reduce this shielding and, thus, to increase the contribution of the lower headgroup layer to the leaflet tension Σ_2.

Inspection of Fig. 7 also shows that the double-peaks of the stress profile within the two head group regions are deformed in a characteristic manner as we increase the lipid density in the upper leaflet. For the latter leaflet, the pressure of the head groups increases and the stress minimum between the two peaks moves towards negative stress values. For the lower leaflet, on the other hand, the head group pressure decreases and the stress minimum between the two peaks moves towards positive stress values and eventually disappears.

Using the stress profiles in Figs. 7 and S2,[50] we determined the spontaneous curvature m using the two computational approaches described in Sec. III. First, we used Eq. (16) and determined the spontaneous curvature m directly via the first moments of these stress profiles. As a result, we obtain the spontaneous curvature m as a function of the asymmetry parameter ϕ_0 as summarized in Table II and plotted in Fig. 8(a). As shown in the latter figure, the spontaneous curvature m is found to increase linearly with the mole fraction ϕ_0 of the lipids in the upper leaflet, as one would expect intuitively.

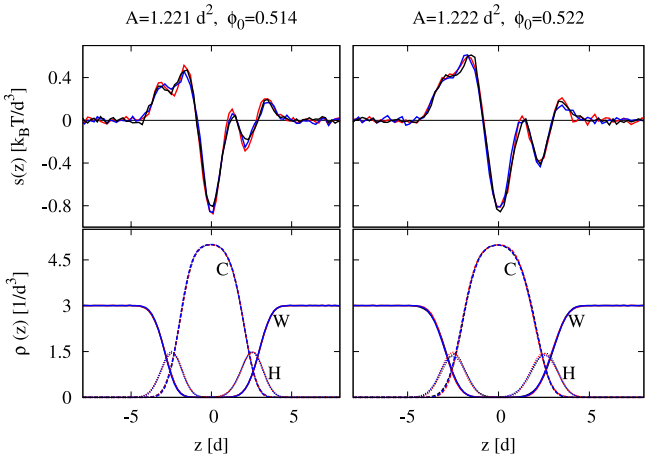

FIG. 7. Stress profiles $s(z)$ (upper panels) and density profiles for water (W), lipid head (H), and lipid chain (C) beads (lower panels) of two asymmetric and tensionless bilayers, which differ in their projected area per lipid, A, and the adjusted mole fraction $\phi = \phi_0$. The blue, red, and black lines correspond to the box height $L_z = 32\,d$, $L_z = 40\,d$, and $L_z = 48\,d$, respectively.

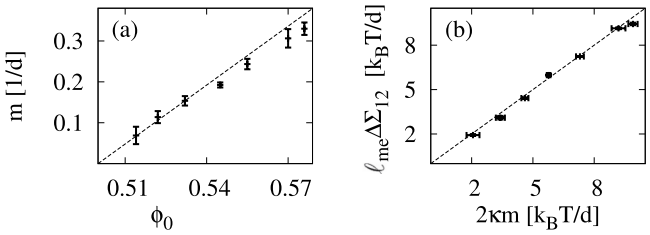

FIG. 8. (a) Spontaneous curvature m of tensionless bilayers as a function of the mole fraction $\phi = \phi_0$. The data points represent the simulation results given in Table II and obtained from the first moment of the stress profiles in Figs. 7 and S2.[50] The dashed line represents a guide to the eye; and (b) comparison of the parameter combination $\ell_{\rm me}\,\Delta\Sigma_{21} \equiv \frac{1}{2}\,\ell_{\rm me}(\delta\Sigma_2 - \delta\Sigma_1)$ as obtained from the excess tensions, see Eq. (36) with $\ell_{\rm me} \equiv 2\ell_{\rm sy}$, with the product $2\kappa m$ as computed from the first moment of the stress profile via Eq. (16). The effective membrane thickness $\ell_{\rm me}$ of the symmetric reference state is found to be $\ell_{\rm me} \simeq 4\,d \simeq 3.2$ nm.

C. Spontaneous curvature from leaflet parameters

We now estimate the spontaneous curvature via the leaflet parameters as described in Secs. III C and III D. We expand the leaflet parameters around the symmetric and tensionless reference state as studied in Sec. II C and denote the corresponding stress profile by $s_{{\rm sy},0}(z)$. The stress profile $s_0(z)$ of the asymmetric and tensionless bilayers considered here is then decomposed according to

$$s_0(z) = s_{{\rm sy},0}(z) + \delta s_0(z), \tag{39}$$

where the deviation $\delta s_0(z)$ vanishes in the limit of small asymmetries. As a result, we obtain the excess tensions

$$\delta\Sigma_1 = \int_0^{L_z/2} {\rm d}z\,\delta s_0(z) = \int_0^{L_z/2} {\rm d}z\,s_0(z) = \Sigma_1 \tag{40}$$

and

$$\delta\Sigma_2 = \int_{-L_z/2}^{0} {\rm d}z\,\delta s_0(z) = \int_{-L_z/2}^{0} {\rm d}z\,s_0(z) = \Sigma_2, \tag{41}$$

where the second equalities follow from Eq. (31).

Because the reference state is provided by a symmetric and tensionless membrane with $\Sigma_{\rm sy} = 0$, the second term on the right hand side of Eq. (35) vanishes and we obtain the asymptotic equality (36) between the product $2\kappa m$ and the parameter combination $\frac{1}{2}\,\ell_{\rm me}(\delta\Sigma_2 - \delta\Sigma_1)$ with the effective membrane thickness $\ell_{\rm me} \equiv 2\ell_{\rm sy}$ of the symmetric reference state. As shown in Fig. 8(b), very good agreement between this parameter combination and the product $2\kappa m$ as calculated from the first moment of the stress profile, see Eq. (16), is obtained for the effective membrane thickness $\ell_{\rm me} \simeq 4\,d \simeq 3.2$ nm.

D. Magnitude of spontaneous curvature

In Table II, the spontaneous curvature m is given in units of $1/d$ because the bead diameter d represents the basic length scale. As explained above, this length scale is estimated to be $d = \ell_{\rm me}/5 = 0.8$ nm using the typical value 4 nm for the separation of the two head group layers. The spontaneous curvature m in Table II then varies from $1/(2.9\,\ell_{\rm me}) = 1/(11.6\text{ nm})$ (top row) to $1/(0.6\,\ell_{\rm me}) = 1/(2.4\text{ nm})$ (bottom row). The smaller value $1/(2.9\,\ell_{\rm me})$ is physically meaningful whereas the larger value $1/(0.5\,\ell_{\rm me})$ is too large because the membrane cannot attain

This article is copyrighted as indicated in the article. Reuse of AIP content is subject to the terms at: http://scitation.aip.org/termsconditions. Downloaded to IP: 141.14.232.254 On: Tue, 03 Feb 2015 17:28:05

a mean curvature of the order of $1/(0.6\,\ell_{\rm me})$ without severely distorting its bilayer structure. If we assume that the membrane can attain mean curvatures up to $1/\ell_{\rm me}$ and if we allow the bilayer to curve towards both sides, Table II implies that the physically meaningful range for the asymmetry parameter ϕ_0 as defined by Eq. (37) is given by $0.468 \lesssim \phi_0 \lesssim 0.532$. It would be instructive to study the free energy barriers for flip flops as a function of ϕ_0 but such a study would be computationally expensive and has not been attempted here.

V. BILAYERS EXPOSED TO ADSORBING PARTICLES

A. Single bilayers with symmetric adsorption

In order to study the spontaneous curvature induced by adsorbing particles, we first consider a symmetric reference system as provided by a single bilayer and small molecules or "particles" that adsorb onto this bilayer, see Fig. 9. The adsorbate particles are represented as single DPD beads, denoted by P in Table I. The DPD interaction parameters for the adsorbate beads are chosen in such a way that these beads localize preferentially at the lipid head groups.

We performed DPD simulations for different numbers of the adsorbate particles corresponding to different bulk concentrations, C, of these particles far away from the bilayer. As before, we used a simulation box that had the dimensions $L_x = L_y = L_z = 32\,d$, and the bilayer spanned the box in the x- and y-directions. As a consequence, the projected area per lipid, A, was also kept constant and had the value $A = 1.23\,d^2$. In addition, for each bulk concentration C of the adsorbate particles, we adjusted the water densities in such a way that the bulk pressure P and thus the normal pressure component $P_{\rm N}$ had the constant value $P_{\rm N} = P = 20.7\,kT/d^3$, as for pure water at standard DPD conditions, see Fig. S3,[50] which displays the number of W beads as a function of the number of P beads. In this way, we varied the adsorbate concentration C keeping the normal pressure $P_{\rm N}$ constant as shown in Fig. 10(a). The latter figure covers the concentration range $0.01/d^3 \lesssim C \lesssim 0.1/d^3$. Using the value $d \simeq 0.8$ nm for the bead diameter, this range corresponds to the molar concentration range 32 mM $\lesssim C \lesssim$ 320 mM which is physically meaningful.

Several density profiles $\rho_{\rm P}(z)$ of the adsorbate particles, corresponding to different values of the bulk concentration C of the adsorbate, are depicted in Fig. 10(b). We note that these densities are much smaller than the overall bead density away from the membrane, which was always close to $\rho = 3/d^3$ irrespective of the adsorbate particle concentration C. In Fig. 10(d), we display the density profiles for the W, H, and C beads. The water density profile away from the bilayer is slightly reduced as we increase the particle concentration but both the H bead and the C bead density remain practically unchanged for all particle concentrations C considered here.

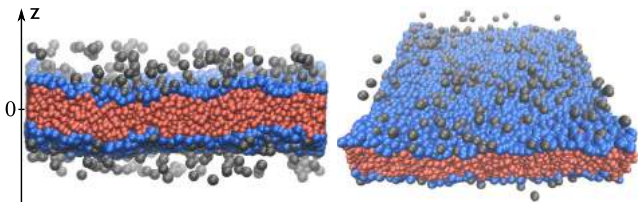

FIG. 9. Simulation snapshots of a lipid bilayer in the presence of small adsorbate particles (gray beads). Lipid head groups are shown in blue and lipid chains in red. The water beads are transparent and not visible. The bilayer consists of $N = 1664$ lipids, which are in contact with 2041 adsorbate particles. As in Fig. 6, the maximum value of the lipid chain (C) density defines the origin of the z-coordinate and the mean curvature is taken to be positive if the bilayer bulges towards the upper leaflet.

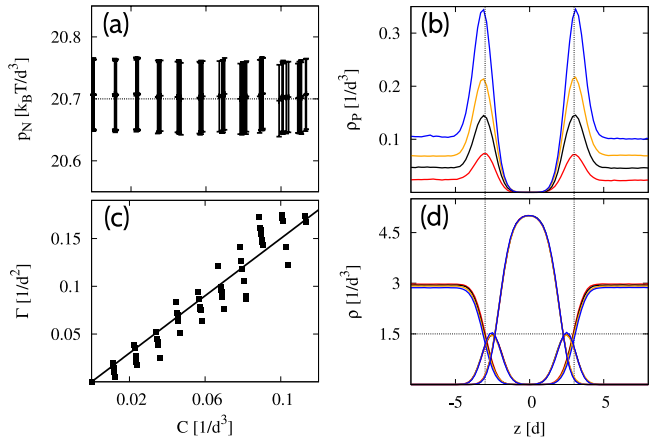

FIG. 10. Symmetric adsorption of small particles onto a symmetric bilayer: (a) The normal pressure component P_N has the constant value $P_N = 20.7\,kT/d^3$, irrespective of the bulk concentration C of the adsorbate particles; (b) density profiles of the adsorbate particles for C = 0.023, 0.046, 0.069, and $0.101/d^3$ (bottom to top). These profiles directly demonstrate that the particles adsorb at the two leaflet-water interfaces; (c) adsorbate coverage Γ as a function of C, calculated from the particle density profiles $\rho_{\rm P}(z)$ via Eq. (42); and (d) density profiles of water (W), head groups (H), and lipid chains (C) for the different concentrations C corresponding to panel (b). The bulk water density is slightly reduced with increasing C but the H and C density profiles remain practically unchanged.

B. Leaflet coverage and leaflet tension

Because of the periodic boundary conditions in the z-direction, we may shift the z-coordinate in such a way that the simulation box is located at $0 < z < L_z$ and view the system as a slab with thickness L_z with one leaflet at $z \gtrsim 0$ and the other leaflet at $z \lesssim L_z$. The density profile $\rho_{\rm P}(z)$ then satisfies the symmetry relation $\rho_{\rm P}(L-z) = \rho_{\rm P}(z)$.

The coverage Γ of the leaflets by the adsorbate particles describes the deviation of the actual particle density $\rho_{\rm P}(z)$ from its bulk value C. Because of the symmetry of the system, each leaflet has the same coverage as given by

$$\Gamma = \tfrac{1}{2}\int_0^{L_z} {\rm d}z\,[\rho_{\rm P}(z) - C]. \tag{42}$$

This coverage vanishes for a uniform profile with $\rho_{\rm P}(z) = C$ and becomes independent of L_z for large L_z (as long as the deviation $\rho_{\rm P}(z) - C$ decays to zero faster than $1/z$ for large z). The dependence of the coverage Γ on the bulk concentration C is shown in Fig. 10(c); the coverage increases linearly with C as expected for small values of C. Therefore, the data follow the linear relation

$$\Gamma = \Gamma_0' C \quad \text{with} \quad \Gamma_0' \equiv \left.\frac{d\Gamma}{dC}\right|_{C=0} \tag{43}$$

over the whole range of concentrations C explored in the simulations. In Fig. 10(c), the coverage Γ is smaller than $0.2/d^2$,

This article is copyrighted as indicated in the article. Reuse of AIP content is subject to the terms at: http://scitation.aip.org/termsconditions. Downloaded to IP: 141.14.232.254 On: Tue, 03 Feb 2015 17:28:05

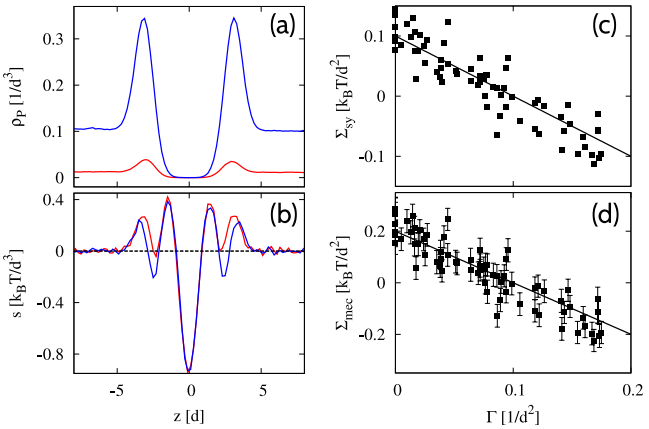

FIG. 11. Symmetric adsorption of small particles onto a symmetric bilayer: (a) Density profiles of the adsorbate particles for $C = 0.012/d^3$ (lower red curve) and $0.101/d^3$ (upper blue curve); (b) stress profiles for the same two concentration values (more negative stress profile for larger concentration); (c) leaflet tension Σ_{sy} as defined by Eq. (44) as a function of coverage Γ. The solid line represents the relationship $\Sigma_{sy}(\Gamma) = \Sigma_{sy}(0) - k_BT\,\Gamma$ as given by Eq. (45); and (d) mechanical tension Σ_{mec} as a function of Γ. The solid line corresponds to $\Sigma_{mec}(\Gamma) = 2\,\Sigma_{sy}(0) - 2k_BT\,\Gamma$. In order to estimate the error bars for the mechanical tension, this quantity has been recorded every 50 DPD steps. Note that the tensionless reference state is obtained for finite coverage $\Gamma = \Gamma_0 \simeq 0.1/d^3$. The corresponding particle density profile is given by the upper blue curve in panel (a). For $\Gamma > \Gamma_0$, the mechanical tension Σ_{mec} is negative and the bilayer membrane is compressed by the adsorbate particles.

which implies that the average separation of the adsorbed particles on one of the membrane leaflets is larger than $2.2\,d$. Therefore, the whole Γ-range displayed in Fig. 10(c) is physically meaningful.

Two examples for the particle density ρ_P and the corresponding stress profile $s_{sy}(z,\Gamma)$ are shown in Figs. 11(a) and 11(b). Because symmetric adsorption implies $s_{sy}(-z,\Gamma) = s_{sy}(z,\Gamma)$, the leaflet tensions $\Sigma_1(\Gamma)$ and $\Sigma_2(\Gamma)$ as defined by Eq. (26) have the same value as given by

$$\Sigma_{sy}(\Gamma) = \tfrac{1}{2}\int_{-L_z/2}^{L_z/2} \mathrm{d}z\; s_{sy}(z,\Gamma). \tag{44}$$

The dependence of the leaflet tension Σ_{sy} on the coverage Γ is displayed in Fig. 11(c). The data in this figure are in good agreement with the linear relation

$$\Sigma_{sy}(\Gamma) \approx \Sigma_{sy}(0) - k_BT\,\Gamma \quad \text{for small} \quad \Gamma \tag{45}$$

which was previously derived from the Gibbs adsorption equation $(\partial\Sigma_i/\partial C)_T \approx -k_BT\,\Gamma/C$ for dilute solutions of the adsorbate particles.[6] Indeed, if we use this latter equation for $\Sigma_i = \Sigma_{sy}$ together with Eq. (43), we obtain the linear relation in Eq. (45). Furthermore, because the mechanical tension $\Sigma_{mec}(\Gamma) = \Sigma_1(\Gamma) + \Sigma_2(\Gamma) = 2\,\Sigma_{sy}(\Gamma)$, we also have $\Sigma_{mec}(\Gamma) \approx 2\,\Sigma_{sy}(0) - 2k_BT\,\Gamma$ for small Γ as shown in Fig. 11(d). Thus, we conclude that the Gibbs adsorption equation applies to the derivatives $(\partial\Sigma_i/\partial C)_T$ of the mechanical leaflet tensions Σ_i as defined in Eq. (26).

C. Two bilayers with asymmetric adsorption

So far, we have discussed symmetric membrane-adsorbate systems for which the adsorbing particles have the same concentration on both sides of the bilayer membrane. The latter geometry is easy to simulate: we only need one bilayer immersed in a single water compartment, which is then in contact with both leaflet-water interfaces because of the periodic boundary conditions in the z-direction. We now turn to a somewhat more complex situation in which the two leaflet-water interfaces are exposed to different concentrations C_{ex} and C_{in} of the adsorbate particles.

1. Simulation box and concentration differences

In order to simulate such asymmetric lipid-adsorbate systems, we introduce a new simulation protocol based on two lipid bilayers that partition the simulation box into two separate compartments with two different particle concentrations, see Fig. 12. The two compartments have equal volumes but contain different numbers of adsorbing particles. Both bilayers are, on average, parallel and span the simulation box in the x- and y-directions. We use the same sign convention for the mean curvature of both the upper and the lower bilayer: they both have positive mean curvature when they bulge towards their own upper leaflet.

Because of the periodic boundary condition in the z-direction, both bilayers are exposed to the same asymmetric environment, see Fig. 12. More precisely, both the lower leaflet of the lower bilayer $\mathcal{B}^{low}$ and the upper leaflet of the upper bilayer $\mathcal{B}^{upp}$ are exposed to the "exterior" particle concentration C_{ex} whereas both the upper leaflet of the lower bilayer $\mathcal{B}^{low}$ and the lower leaflet of the upper bilayer $\mathcal{B}^{upp}$ are exposed to the "interior" particle concentration C_{in}. We then define the concentration difference ΔC by

$$\Delta C = \Delta C^{upp} \equiv C_{ex} - C_{in} \quad \text{for bilayer } \mathcal{B}^{upp} \tag{46}$$

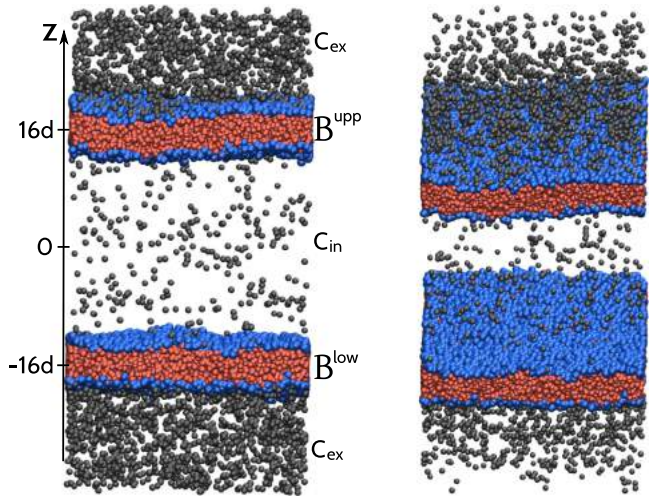

FIG. 12. Simulation snapshots (side view and oblique view) of two bilayers, the lower bilayer $\mathcal{B}^{low}$ and the upper one $\mathcal{B}^{upp}$, exposed to two aqueous solutions with particle concentrations C_{ex} and C_{in}. The lower leaflet of bilayer $\mathcal{B}^{low}$ is exposed to the same particle concentration as the upper leaflet of bilayer $\mathcal{B}^{upp}$ and vice versa. The simulation box extends from $z = -32\,d$ to $z = 32\,d$. The midplane of the lower bilayer is located at $z = -16\,d$, the midplane of the upper one at $z = 16\,d$. Thus, the two bilayers partition the simulation box into two compartments of equal volume. For each bilayer, the mean curvature is taken to be positive if the bilayer bulges towards its upper leaflet, i.e., towards the positive z-direction.

This article is copyrighted as indicated in the article. Reuse of AIP content is subject to the terms at: http://scitation.aip.org/termsconditions. Downloaded to IP: 141.14.232.254 On: Tue, 03 Feb 2015 17:28:05

and by

$$\Delta C = \Delta C^{\rm low} \equiv C_{\rm in} - C_{\rm ex} \quad \text{for bilayer } \mathcal{B}^{\rm low}. \tag{47}$$

These definitions are consistent with our convention for the mean curvature of the two bilayers.

For the simulations reported here, the simulation box had the same lateral dimensions $L_x = L_y = 32\,d$ as for the symmetric adsorbate-lipid systems, but the perpendicular dimension was now $L_z = 64\,d$, i.e., twice as large as for the symmetric case. Both bilayers contained the same number $N = 1664$ of lipids corresponding to the same projected area $A = 1.23\,d^2$ per lipid. The water densities were adjusted in such a way that the normal pressure had the standard value $P_N = 20.7 k_B T/d^3$ irrespective of the particle concentrations.

Real lipid bilayers are observed to be essentially impermeable to ions and to all molecules apart from water. Therefore, on the time scales of typical experiments, the concentrations $C_{\rm ex}$ and $C_{\rm in} \neq C_{\rm ex}$ within the exterior and interior compartments can be considered to be constant and time-independent. In order to ensure that this constrained equilibrium also applies to our simulations, we first performed extended simulations of the two-bilayer system for about 2 μs and confirmed that the number of the adsorbing particles remained constant in each aqueous compartment on the time scales of the simulations. We also checked that the special case with identical concentration $C_{\rm ex} = C_{\rm in}$ in the two aqueous compartments reproduced the results for a single bilayer as described in Subsection V A and V B.

2. Tensionless membranes with $C_{\rm ex} \neq C_{\rm in}$

After these initial test runs, we identified and studied pairs of concentrations $C_{\rm ex}$ and $C_{\rm in}$ for which the two membranes experienced very low mechanical tensions. We then determined, for each such concentration pair, the density and stress profiles as illustrated in Fig. 13, where these profiles are displayed for the concentrations $C_{\rm ex} = 0.102/d^3$ and $C_{\rm in} = 0.012/d^3$. The density profiles of the lipid tails and heads, see Fig. 13(a), appear to be unaffected by the presence of the adsorbing particles. The water density away from the bilayers is somewhat smaller than $\rho = 3/d^3$ because of the adsorbing particles in the aqueous compartments and the requirement to keep the normal pressure at its standard value $P_N = 20.7 k_B T/d^3$, see Fig. S3.[50] From the density profile for the adsorbate particles, see Fig. 13(b), we can determine both the bulk concentrations $C_{\rm ex}$ and $C_{\rm in}$ of the adsorbing particles away from the bilayers and the particle coverages of the two leaflets, arising from the increased particle density close to the bilayers. The corresponding stress profile is displayed in Fig. 13(c).

Because both bilayers have the same lateral size and contain the same number of lipid molecules, they experience, on average, the same mechanical tension. We calculated the tension of each bilayer separately by partitioning the simulation box shown in Fig. 12 into two subvolumes of equal size. Each subvolume contained one bilayer and its tension was then obtained by integrating the stress profile over the z-coordinate of the corresponding subvolume, compare Eq. (7).

We considered 16 pairs of concentrations $C_{\rm ex}$ and $C_{\rm in}$ with $C_{\rm ex} > C_{\rm in}$ as depicted in Fig. 14(a). According to Eqs. (46) and (47), the upper bilayer is then exposed to the concentration difference $\Delta C = C_{\rm ex} - C_{\rm in}$ whereas the lower bilayer is exposed to the concentration difference $\Delta C = C_{\rm in} - C_{\rm ex}$. Therefore, the 16 two-bilayer systems provide data for 32 different single bilayers.

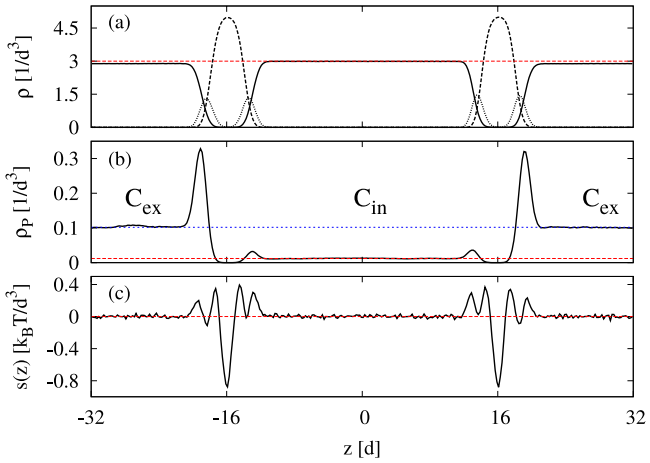

FIG. 13. Density and stress profiles for two bilayer membranes that partition the simulation box into two aqueous compartments with equal volumes but different particle concentrations $C_{\rm ex}$ and $C_{\rm in} < C_{\rm ex}$: (a) Density profiles of water (solid line), lipid chains (dashed line), and lipid heads (dotted line). The water density away from the bilayers is somewhat smaller than $3/d^3$ (horizontal red dashed line) because this density was adjusted in such a way that the water-particle mixture always had the standard normal pressure $P_N = 20.7\,k\,BT/d^3$, see Fig. S3;[50] (b) density profile $\rho_{\rm P}(z)$ of adsorbate particles with the bulk densities $C_{\rm ex} = 0.102/d^3$ and $C_{\rm in} = 0.012/d^3$ as indicated by the horizontal red and blue dashed lines; and (c) lateral stress profile $s(z)$. The adsorbing particles act to increase the pressure within the head group layers and to move the corresponding double-peak structure of the stress profile towards negative stress values. In this example, the left bilayer $\mathcal{B}^{\rm low}$ and the right bilayer $\mathcal{B}^{\rm upp}$ experience the mechanical tension $\Sigma_{\rm mec} = (0.08 \pm 0.06)\,k_B T/d^2$ and $\Sigma_{\rm mec} = (0.07 \pm 0.06)\,k_B T/d^2$, respectively.

For each concentration pair, we performed eight simulation runs of 2 μs and, thus, studied the corresponding two-

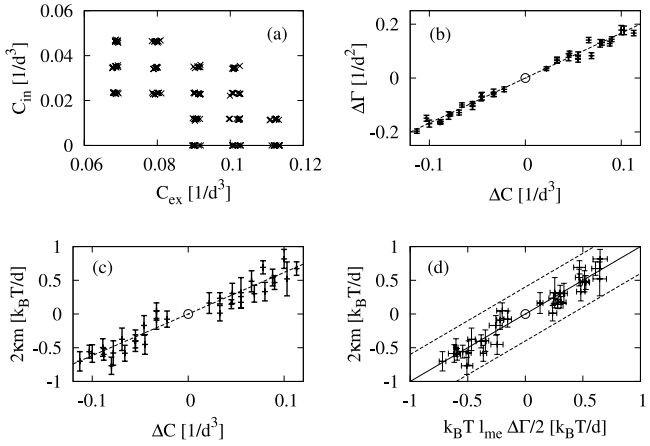

FIG. 14. Asymmetric adsorption of particles onto bilayer membranes: (a) Concentrations $C_{\rm ex}$ and $C_{\rm in}$ for which the density and stress profiles have been computed; (b) coverage difference $\Delta\Gamma$ and (c) the product $2\kappa m$ as a function of concentration difference ΔC. The coverage difference was obtained by integration of the particle density, the product $2\kappa m$ from the first moment of the stress profile, see main text; and (d) the product $Y \equiv 2\kappa m$ as obtained from the stress profile plotted against the parameter combination $X \equiv \frac{1}{2}\,k_B T\,\ell_{\rm me}\Delta\Gamma$ with effective membrane thickness $\ell_{\rm me} = 2\ell_{\rm sy} = 7.2\,d$, see Eq. (59). The dashed line represents the diagonal line $Y = X$, the dotted lines are shifted lines with $Y = X \pm 0.5$.

This article is copyrighted as indicated in the article. Reuse of AIP content is subject to the terms at: http://scitation.aip.org/termsconditions. Downloaded to IP: 141.14.232.254 On: Tue, 03 Feb 2015 17:28:05

bilayer system for a total run time of 16 μs. For each run, we determined the mechanical tensions $\Sigma_{\rm mec}^{\rm low}$ and $\Sigma_{\rm mec}^{\rm upp}$ of the two bilayers $\mathcal{B}^{\rm low}$ and $\mathcal{B}^{\rm upp}$ from the stress profiles in the two subvolumes. We selected those runs for which both bilayers were tensionless in the sense that their mechanical tensions satisfied $-0.1\,k_{\rm B}T/d^2 < \Sigma_{\rm mec}^{\rm low} < 0.1\,k_{\rm B}T/d^2$ and $-0.1\,k_{\rm B}T/d^2 < \Sigma_{\rm mec}^{\rm upp} < 0.1\,k_{\rm B}T/d^2$. For all concentration pairs, the latter condition applied to at least four of the eight simulation runs.

3. Coverage differences $\Delta\Gamma$ between the two leaflets

The selected runs with two tensionless bilayers were then used to calculate the coverages $\Gamma_i^{\rm low}$ and $\Gamma_i^{\rm upp}$ with $i = 1, 2$ for the four leaflets of the two bilayers in Fig. 12. Because of the periodic boundary conditions, we have the identities

$$\Gamma_1^{\rm upp} = \Gamma_2^{\rm low} \equiv \Gamma_{\rm ex} \tag{48}$$

and

$$\Gamma_1^{\rm low} = \Gamma_2^{\rm upp} \equiv \Gamma_{\rm in}. \tag{49}$$

The different coverages were calculated from the particle density profiles within the two subvolumes using Eq. (42) with integration limits as given by the midplanes of the two bilayers. We then defined the coverage differences

$$\Delta\Gamma = \Delta\Gamma^{\rm upp} \equiv \Gamma_1^{\rm upp} - \Gamma_2^{\rm upp} = \Gamma_{\rm ex} - \Gamma_{\rm in} \quad \text{for } \mathcal{B}^{\rm upp} \tag{50}$$

and

$$\Delta\Gamma = \Delta\Gamma^{\rm low} \equiv \Gamma_1^{\rm low} - \Gamma_2^{\rm low} = \Gamma_{\rm in} - \Gamma_{\rm ex} \quad \text{for } \mathcal{B}^{\rm low} \tag{51}$$

in accordance with our sign convention for the mean curvature of the two bilayers and with the definition of the concentration difference ΔC in Eqs. (46) and (47).

In Fig. 14(b), the coverage difference $\Delta\Gamma$ as defined by Eqs. (50) and (51) is plotted against the concentration difference ΔC as defined by Eqs. (46) and (47). Inspection of this figure shows that both quantities are linearly related over the whole range of ΔC-values that has been studied here. As shown in Fig. 14(b), the explored range of concentration differences ΔC varied from $-0.1/d^3 \lesssim \Delta C \lesssim +0.1/d^3$ which is equivalent, for bead diameter $d \simeq 0.8$ nm, to the molar concentration range -320 mM $\lesssim \Delta C \lesssim +320$ mM.

4. Spontaneous curvature from stress profile

For a single bilayer with vanishing mechanical tension, the first moment $\int {\rm d}z\, s(z) z$ of the stress profile $s(z)$ is proportional to the spontaneous curvature m, see Eq. (16). For the two bilayer systems in Fig. 12, the up-down asymmetry of the upper bilayer is opposite to the up-down asymmetry of the lower bilayer, see Fig. 13. Therefore, for a "tensionless" two-bilayer system, the first moment $\int {\rm d}z\, s(z) z$ of the stress profile $s(z)$ vanishes if the integral is taken over the whole simulation box, and we have to integrate over only half the box in order to determine the spontaneous curvature of a single bilayer.

Thus, we determined the spontaneous curvatures $m^{\rm upp}$ and $m^{\rm low}$ of the upper and lower bilayer via

$$2\kappa m^{\rm upp} = -\int_0^{32d} {\rm d}z\, s(z)\, z \tag{52}$$

and

$$2\kappa m^{\rm low} = -\int_{-32d}^{0} {\rm d}z\, s(z)\, z, \tag{53}$$

compare Fig. 13. The result of these calculations is displayed in Fig. 14(c) where the negative and positive values of m were obtained for the lower and upper bilayers, $\mathcal{B}^{\rm low}$ and $\mathcal{B}^{\rm upp}$, respectively. The data in Fig. 14(c) are more noisy than those in Fig. 14(b) reflecting the deviations of the low but nonzero mechanical tensions $\Sigma_{\rm mec}$ from $\Sigma_{\rm mec} = 0$, but the relationship between $2\kappa m$ and ΔC is clearly linear again.

5. Spontaneous curvature from leaflet parameters

Next, we again estimate the spontaneous curvatures of the bilayers via the leaflet parameters as described in Secs. III C and III D. For notational simplicity, we discuss only the upper bilayer $\mathcal{B}^{\rm upp}$ and suppress the superscript "upp" in this subsection. We start from the stress profiles $s_{\rm sy}(z,\Gamma)$ for symmetric adsorption as introduced in Sec. V B. Inspection of Figs. 11(c) and 11(d) shows that the mechanical tension $\Sigma_{\rm mec}$ vanishes for a certain, intermediate coverage $\Gamma = \Gamma_0 \simeq 0.1/d^2$. We now take the corresponding stress profile $s_{\rm sy}(z,\Gamma_0)$ as our symmetric and tensionless reference state. The stress profile of the asymmetric and tensionless upper bilayer is decomposed according to

$$s_1(z,\Gamma_1) = s_{\rm sy}(z,\Gamma_0) + \delta s_1(z,\Gamma_1) \quad \text{for } 16\,d < z < 32\,d \tag{54}$$

and

$$s_2(z,\Gamma_2) = s_{\rm sy}(z,\Gamma_0) + \delta s_2(z,\Gamma_2) \quad \text{for } 0 < z < 16\,d, \tag{55}$$

where the profiles $\delta s_1(z,\Gamma_1)$ and $\delta s_2(z,\Gamma_2)$ vanish in the limit of small $\Gamma_1 - \Gamma_0$ and small $\Gamma_0 - \Gamma_2$, respectively. We then obtain the excess tensions

$$\delta\Sigma_1(\Gamma_1) = \int_{16d}^{32d} {\rm d}z\, \delta s_1(z,\Gamma_1) = \int_{16d}^{32d} {\rm d}z\, s_1(z,\Gamma_1) = \Sigma_1(\Gamma_1) \tag{56}$$

and

$$\delta\Sigma_2(\Gamma_2) = \int_{0}^{16d} {\rm d}z\, \delta s_2(z,\Gamma_2) = \int_{0}^{16d} {\rm d}z\, s_2(z,\Gamma_2) = \Sigma_2(\Gamma_2), \tag{57}$$

where the second equalities follow from

$$\Sigma_{\rm sy} = \int_0^{16d} {\rm d}z\, s_{\rm sy}(z,\Gamma_0) = \int_{16d}^{32d} {\rm d}z\, s_{\rm sy}(z,\Gamma_0) = 0$$

as in Eq. (31).

Because the reference state is provided by a symmetric and tensionless bilayer with $\Sigma_{\rm sy} = 0$, the second term on the right hand side of Eq. (35) vanishes and the asymptotic equality in Eq. (36) with $\ell_{\rm sy} = \frac{1}{2}\,\ell_{\rm me}$ now becomes

$$2\kappa m \approx \tfrac{1}{2}\,\ell_{\rm me}[\delta\Sigma_2(\Gamma_2) - \delta\Sigma_1(\Gamma_1)]. \tag{58}$$

Using the equalities $\delta\Sigma_i(\Gamma_i) = \Sigma_i(\Gamma_i)$ and the linear relationships $\Sigma_i(\Gamma_i) \approx \Sigma_i(0) - k_{\rm B}T\Gamma_i$ as in Eq. (45) with $\Sigma_1(0) = \Sigma_2(0) = \Sigma_{\rm sy}(0)$, we can rewrite Eq. (58) in the more transparent form

$$2\kappa m \approx \tfrac{1}{2}\; k_{\rm B}T\ell_{\rm me}\,(\Gamma_1 - \Gamma_2) = \tfrac{1}{2}\; k_{\rm B}T\,\ell_{\rm me}\,\Delta\Gamma \tag{59}$$

as previously derived in Ref. 6. In order to scrutinize this relationship, we now combine the data in Fig. 14(b) and 14(c) and plot the quantity $2\kappa m$ as calculated from the first moment of the

This article is copyrighted as indicated in the article. Reuse of AIP content is subject to the terms at: http://scitation.aip.org/termsconditions. Downloaded to IP: 141.14.232.254 On: Tue, 03 Feb 2015 17:28:05

stress profile against the parameter combination $\frac{1}{2}\, k_B T \ell_{me} \Delta\Gamma$ using the coverage $\Delta\Gamma$ as computed from the particle density profile. The best agreement between these two quantities is obtained for the effective membrane thickness $\ell_{me} = 7.2\, d \simeq 5.8$ nm. It is important to note that this effective thickness applies to a symmetric and tensionless bilayer with the same particle coverage $\Gamma_0 \simeq 0.1/d^2$ on both leaflets, see Fig. 11(d). Note also that the specific value $\ell_{me} \simeq 7.2\, d$ found here applies to a certain particle size and to certain intermolecular interactions of the particles with water and lipid molecules. In general, the effective membrane thickness is expected to vary as we change these parameters of the adsorbing particles.

6. Magnitude of spontaneous curvature

The product $2\kappa m$ as depicted in Fig. 14(c) and 14(d) varies in the range $-k_B T/d \lesssim 2\kappa m \lesssim +k_B T/d$. Using the bead diameter $d = \ell_{me}/5 \simeq 0.8$ nm and the bending stiffness $\kappa \simeq 15 k_B T$, we obtain the physically meaningful range $-(1/24\ \text{nm}) \lesssim m \lesssim +(1/24\ \text{nm})$ for the spontaneous curvature m as induced by asymmetric adsorption for the adsorbate particles considered in this study.

VI. SUMMARY AND OUTLOOK

In the present paper, we have used coarse-grained molecular dynamics simulations to determine the spontaneous curvature of bilayer membranes. We considered two mechanisms for the generation of spontaneous curvature: (i) different lipid densities within the two leaflets were studied in Sec. IV and (ii) leaflets exposed to different concentrations of adsorbing particles, which may be ions, small molecules, or peptides, were discussed in Sec. V C.

In both cases, we used two computational methods to determine the spontaneous curvature. The first method uses the relation (16) between the spontaneous curvature m and the first moment of the stress profile across the bilayer membrane.[31–33] This relation relies on detailed knowledge about the complex structure of the stress profile. The other method starts from the intuitive view that the two leaflet-water interfaces can be characterized by certain leaflet tensions, Σ_1 and Σ_2, which we defined here in terms of the mechanical tensions within the two leaflets. The sum of these two leaflet tensions is equal to the mechanical tension of the whole bilayer, see Eqs. (26) and (27). Expanding the leaflet parameters around symmetric and tensionless states, we then arrive at the linear relationship (36) between the spontaneous curvature and the excess tensions $\delta\Sigma_i$ of the two leaflets. It is important to note that these excess tensions are defined for the planar state of the membrane and are, thus, accessible to simulations with periodic boundary conditions.

The relationship (36) involves the effective membrane thickness of the symmetric and tensionless reference state. For asymmetric lipid densities in the two leaflets of the bilayer, we found the effective membrane thickness $\ell_{me} = 4\, d \simeq 3.2$ nm, see Fig. 8(b). For asymmetric adsorption of a certain species of adsorbing particles, we obtained the effective membrane thickness $\ell_{me} = 7.2\, d \simeq 5.8$ nm, see Fig. 14(d). In the latter case, the symmetric reference state is already covered by adsorbing particles leading to the coverage $\Gamma_0 \simeq 0.1/d^2$ as in Fig. 11. We thus conclude that the two computational methods, which were based on two different views about the molecular mechanism for spontaneous curvature generation, are completely consistent with each other.

For bilayers with asymmetric lipid densities, our main results are summarized in Table II and Fig. 8. In Fig. 8(a), the spontaneous curvature is plotted as a function of the lipid asymmetry ϕ_0 which describes the mole fraction of lipid molecules within the upper leaflet of tensionless bilayers. A symmetric bilayer with vanishing spontaneous curvature is described by $\phi_0 = 1/2$. The physically meaningful range of the control parameter ϕ_0 is provided by $0.468 < \phi_0 < 0.532$ for which the spontaneous curvature varies from $-1/\ell_{me} \lesssim m \lesssim +1/\ell_{me}$.

For symmetric adsorption, i.e., for bilayers exposed to two aqueous solutions with equal adsorbate concentrations C_{ex} and C_{in} on both sides of the bilayers, the leaflet tensions Σ_1 and Σ_2 are equal and decrease linearly with increasing coverage of the adsorbate particles, see Fig. 11(c) and Eq. (42), as derived in Ref. 6 from the Gibbs adsorption equation. Thus, we conclude that the Gibbs adsorption equation applies to the adsorption onto the bilayer leaflets provided one considers the derivatives $(\partial\Sigma_i/\partial C)_T$ of the mechanical leaflet tensions Σ_i as defined in Eq. (26).

In order to study bilayers exposed to different adsorbate concentrations C_{ex} and C_{in}, we introduced a novel simulation protocol based on two bilayers separated by two aqueous compartments with different adsorbate concentrations, see Fig. 12. We used this system to explore concentration differences ΔC within the molar concentration range -320 mM $\lesssim \Delta C \lesssim +320$ mM. The main results for these systems with asymmetric adsorption are displayed in Fig. 14. The functional dependence of the spontaneous curvature on the concentration difference ΔC is shown in Fig. 14(c), the agreement between the two computational methods in Fig. 14(d). Our simulation results confirm the linear relation between spontaneous curvature and coverage asymmetry $\Delta\Gamma$, described by Eq. (59) and predicted in Ref. 6. These results also demonstrate that rather small adsorbate particles with a size below 1 nm can generate large spontaneous curvatures m in the range $-(1/24\ \text{nm}) \lesssim m \lesssim +(1/24\ \text{nm})$.

The relationship (59) between the spontaneous curvature and the coverage of the adsorbate particles does not involve the stress profile but only the effective membrane thickness ℓ_{me}. For spherical particles of size d as studied here, this thickness ℓ_{me} was found to be $7.2\, d$ which is quite close to what one would expect naively. Indeed, in the absence of the adsorbate particles, the separation of the two head group layers is $5\, d$ as in Fig. 3(a). A monolayer of adsorbate particles has a thickness comparable to the size of the particles. For spherical particles with diameter d, the thickness ℓ_{me} of a membrane with two layers of adsorbate particles is then expected to be about $5\, d + 2\, d = 7\, d$.

Using the relationship (59) for asymmetric adsorption, one can deduce the spontaneous curvature from a naive estimate of the membrane thickness ℓ_{me} together with some data on the adsorbate coverages Γ_1 and Γ_2. Such a deduction method that does not involve the stress profile is quite valuable from

This article is copyrighted as indicated in the article. Reuse of AIP content is subject to the terms at: http://scitation.aip.org/termsconditions. Downloaded to IP: 141.14.232.254 On: Tue, 03 Feb 2015 17:28:05

an experimental point of view because, with available experimental techniques, one can measure the coverages but not the stress profiles. Furthermore, the simulation data in Fig. 14 imply that, depending on the bulk concentrations of the adsorbate particles, the spontaneous curvature m can vary over three orders of magnitude from about 1/(20 nm) down to the inverse size of giant vesicles, which is of the order of $1/(20\ \mu\text{m})$. Because of this large range of possible m-values, the deduction method based on Eq. (59) is quite useful even if the naive estimate of the membrane thickness involves an uncertainty of 10% or 20%.

Our simulation protocol for calculating the spontaneous curvature induced by asymmetric adsorption is quite general and can be applied to any molecular model of the lipid/adsorbate system. In particular, it can be applied to atomistic simulations of specific lipids and specific ions or peptides that adsorb onto the bilayers. Using our protocol, one could also study the asymmetric adsorption of Bin/Amphiphysin/Rvs (BAR)-domain proteins or other rigid macromolecules that bind to membranes and generate local membrane curvature via their molecular shape. One now has to distinguish this local, protein-induced curvature from the spontaneous curvature which governs the membrane shape on larger length scales and depends both on the local, protein-induced curvature and on the coverage by the adsorbed proteins.[51,52] Thus, to determine the spontaneous curvature induced by BAR-domains or other macromolecules will be computationally demanding because one should simulate membrane segments that are large compared to the average separation between the adsorbed proteins or macromolecules.

Our protocol can be easily extended to other mechanisms for spontaneous curvature generation such as (i) to lipid bilayers with different lipid species and compositional asymmetries between the two leaflets and (ii) to solute particles that form depletion layers in front of the leaflet-water interfaces. As shown in Ref. 5, such depletion layers should also induce a spontaneous curvature. Likewise, analytical theories have recently predicted that the spontaneous curvature has a strong effect on the engulfment of nanoparticles,[53] another process that can be studied by molecular simulations.[54–58] Finally, because of recent experimental developments,[16,59] it now seems feasible to measure the spontaneous curvatures induced by ions, small molecules, or peptides using fluorescence microscopy of giant unilamellar vesicles.

ACKNOWLEDGMENTS

We thank Julian Shillcock and Jinglei Hu for helpful discussions. The work of B.R. has been supported by the Ministry of Science and Higher Education of Poland Grant No. IP2012 0383 72.

NOMENCLATURE

A	projected area per lipid molecule.
A_0	molecular area of tensionless membrane.
$\mathcal{A}$	membrane area.
$\mathcal{A}_1$	area of upper-leaflet-water interface.
$\mathcal{A}_2$	area of lower-leaflet-water interface.
a_{ij}	DPD force parameter.
$\mathcal{B}^{\text{low}}$	lower bilayer membrane.
$\mathcal{B}^{\text{upp}}$	upper bilayer membrane.
C	lipid chain bead.
C	concentration of adsorbate particles.
C_{ex}	concentration within exterior compartment.
C_{in}	concentration within interior compartment.
C_1,C_2	two principal curvatures of membrane surface.
d	bead diameter.
$\Delta\mathcal{F}_{\text{int}}$	change in interfacial free energy.
$\Delta\Gamma$	difference in adsorbate coverage.
$\delta\Sigma_1$	excess tension within upper leaflet.
$\delta\Sigma_2$	excess tension within lower leaflet.
$\mathcal{E}_{\text{be}}$	bending energy of membrane.
$\vec{F}_{ij}$	force exerted by particle j onto particle i
$\vec{F}^C_{ij}$	conservative force.
$\vec{F}^D_{ij}$	dissipative force.
$\vec{F}^R_{ij}$	random force.
Γ	adsorbate coverage.
Γ_{ex}	adsorbate coverage from exterior compartment.
Γ_{in}	adsorbate coverage from interior compartment.
Γ_1	adsorbate coverage of upper leaflet.
Γ_2	adsorbate coverage of lower leaflet.
Γ_i^{low}	coverage of leaflet $i = 1,2$ of lower bilayer $\mathcal{B}^{\text{low}}$.
Γ_i^{upp}	coverage of leaflet $i = 1,2$ of upper bilayer $\mathcal{B}^{\text{upp}}$.
H	lipid head bead.
k_{B}	Boltzmann constant.
K_A	area compressibility modulus.
κ	bending rigidity of bilayer membrane.
ℓ_{me}	membrane thickness, $\ell_{\text{me}} = \ell_1 + \ell_2$.
ℓ_1	thickness of upper leaflet.
ℓ_2	thickness of lower leaflet.
L_x,L_y	lateral dimensions of simulation box.
L_z	height of simulation box.
m	spontaneous curvature of membrane.
M	mean curvature of membrane.
N_1	number of lipid molecules in upper leaflet.
N_2	number of lipid molecules in lower leaflet.
P	adsorbate particle bead.
P	bulk pressure.
P_{N}	normal pressure component.
P_{T}	tangential pressure component.
ϕ	mole fraction of upper leaflet.
ϕ_0	mole fraction of tensionless bilayer.
q	wave number of shape fluctuations.
ρ	particle density in the bulk.
$\rho_{\text{P}}(z)$	density profile of adsorbate particles.
$\rho_{\text{W}}(z)$	density profile of water beads.
Σ_{mec}	mechanical tension of bilayer membrane.
Σ_{N}	normal stress component.
Σ_{T}	tangential stress component.
Σ_1	mechanical tension within upper leaflet.
Σ_2	mechanical tension within lower leaflet.
Σ_{sy}	leaflet tension for a symmetric bilayer.
$s(z)$	stress profile.
$s_{\text{sy}}(z)$	stress profile of symmetric bilayer.
$s_{\text{sy},0}(z)$	stress profile of symmetric and tensionless bilayer.
T	temperature.
$\mathcal{T}_{\text{mic}}$	microscopic torque acting on bilayer cross-section.
$\mathcal{T}_{\text{nan}}$	nanoscopic torque acting on neutral surface.
W	water bead.
x,y	coordinates parallel to bilayer.
z	coordinate perpendicular to bilayer.

This article is copyrighted as indicated in the article. Reuse of AIP content is subject to the terms at: http://scitation.aip.org/termsconditions. Downloaded to IP: 141.14.232.254 On: Tue, 03 Feb 2015 17:28:05

[1]*Structure and Dynamics of Membranes*, Handbook of Biological Physics Vol. 1, edited by R. Lipowsky and E. Sackmann (Elsevier, Amsterdam, 1995).
[2]V. Kiessling, C. Wan, and L. K. Tamm, "Domain coupling in asymmetric lipid bilayers," Biochim. Biophys. Acta **1788**, 64–71 (2009).
[3]W. L. Hwang, M. Chen, B. Cronin, M. Holden, and H. Bayley, "Asymmetric droplet interface bilayers," J. Am. Chem. Soc. **130**, 5878–5879 (2008).
[4]S. Chiantia, P. Schwille, A. S. Klymchenko, and E. London, "Asymmetric GUVs prepared by MbCD-mediated lipid exchange: An FCS study," Biophys. J. **100**, L01–L03 (2011).
[5]R. Lipowsky and H. G. Döbereiner, "Vesicles in contact with nanoparticles and colloids," Europhys. Lett. **43**, 219–225 (1998).
[6]R. Lipowsky, "Spontaneous tubulation of membranes and vesicles reveals membrane tension generated by spontaneous curvature," Faraday Discuss. **161**, 305–331 (2013).
[7]K. Takei, V. I. Slepnev, V. Haucke, and P. D. Camilli, "Functional partnership between amphiphysin and dynamin in clathrin-mediated endocytosis," Nat. Cell Biol. **1**, 33–39 (1999).
[8]B. J. Peter, H. M. Kent, I. G. Mills, Y. Vallis, P. J. G. Butler, P. R. Evans, and H. T. McMahon, "BAR domains as sensors of membrane curvature: The amphiphysin BAR structure," Science **303**, 495–499 (2004).
[9]K. Farsad, N. Ringstad, K. Takei, S. R. Floyd, K. Rose, and P. D. Camilli, "Generation of high curvature membranes mediated by direct endophilin bilayer interactions," J. Cell Biol. **155**, 193–200 (2001).
[10]Q. Wang, V. A. S. Navarro, G. Peng, E. Molinelli, S. L. Goh, B. L. Judson, K. R. Rajashankar, and H. Sondermann, "Molecular mechnism of membrane constriction and tubulation mediated by the F-BAR protein Pacsin/Syndapin," Proc. Natl. Acad. Sci. U. S. A. **106**, 12700–12705 (2009).
[11]M. G. J. Ford, I. G. Mills, B. J. Peter, Y. Vallis, G. J. K. Praefcke, P. R. Evans, and H. T. McMahon, "Curvature of clathrin-coated pits driven by epsin," Nature **419**, 361–366 (2002).
[12]Y. A. Domanov and P. K. J. Kinnunen, "Antimicrobial peptides temporins B and L induce formation of tubular lipid protrusions from supported phospholipid bilayers," Biophys. J. **91**, 4427–4439 (2006).
[13]M. Mally, J. Majhenc, S. Svetina, and B. Zeks, "The response of giant phospholipid vesicles to pore-forming peptide melittin," Biochim. Biophys. Acta **1768**, 1179–1189 (2007).
[14]T. M. Domingues, K. A. Riske, and A. Miranda, "Revealing the lytic mechanism of the antimicrobial peptide gomesin by observing giant unilamellar vesicles," Langmuir **26**, 11077–11084 (2010).
[15]A. Arouni, V. Kiessling, L. Tamm, M. Dathe, and A. Blume, "Morphological changes induced by the action of antimicrobial peptides on supported lipid bilayers," J. Phys. Chem. **115**, 158–167 (2011).
[16]Y. Li, R. Lipowsky, and R. Dimova, "Membrane nanotubes induced by aqueous phase separation and stabilized by spontaneous curvature," Proc. Natl. Acad. Sci. U. S. A. **108**, 4731–4736 (2011).
[17]W. D. Bancroft, "The theory of emulsification, V," J. Phys. Chem. **17**, 501–519 (1913).
[18]W. Bancroft and C. Tucker, "Gibbs on emulsification," J. Phys. Chem. **31**, 1681–1692 (1927).
[19]F. C. Frank, "Liquid crystals I: On the theory of liquid crystals," Discuss. Faraday Soc. **25**, 19–28 (1958).
[20]W. Helfrich, "Elastic properties of lipid bilayers: Theory and possible experiments," Z. Naturforsch. **28c**, 693–703 (1973).
[21]R. Goetz and R. Lipowsky, "Computer simulations of bilayer membranes: Self-assembly and interfacial tension," J. Chem. Phys. **108**, 7397–7409 (1998).
[22]J. C. Shillcock and R. Lipowsky, "Equilibrium structure and lateral stress distribution of amphiphilic bilayers from dissipative particle dynamics simulations," J. Chem. Phys. **117**, 5048–5061 (2002).
[23]G. Ayton and G. A. Voth, "Bridging microscopic and mesoscopic simulations of lipid bilayers," Biophys. J. **83**, 3357–3370 (2002).
[24]G. Srinivas, D. E. Discher, and M. L. Klein, "Self-assembly and properties of diblock copolymers by coarse-grain molecular dynamics," Nat. Mater. **3**, 638–644 (2004).
[25]R. Goetz, G. Gompper, and R. Lipowsky, "Mobilitiy and elasticity of self-assembled membranes," Phys. Rev. Lett. **82**, 221–224 (1999).
[26]E. G. Brandt, A. R. Braun, J. N. Sachs, J. F. Nagle, and O. Edholm, "Interpretation of fluctuation spectra in lipid bilayer simulations," Biophys. J. **100**, 2104–2111 (2011).
[27]M. C. Watson, E. S. Penev, P. M. Welch, and F. L. H. Brown, "Thermal fluctuations in shape, thickness, and molecular orientation in lipid bilayers," J. Chem. Phys. **135**, 244701 (2011).
[28]P. Tarazona, E. Chacon, and F. Bresme, "Thermal fluctuations and bending rigidity of bilayer membranes," J. Chem. Phys. **139**, 094902 (2013).
[29]M. Orsi, D. Y. Haubertin, W. E. Sanderson, and J. W. Essex, "A quantitative coarse-grain model for lipid bilayers," J. Phys. Chem. B **112**, 802–815 (2008).
[30]M. Hu, J. J. Briguglio, and M. Deserno, "Determining the Gaussian curvature modulus of lipid membranes in simulations," Biophys. J. **102**, 1403–1410 (2012).
[31]W. Helfrich, "Amphiphilic mesophases made of defects," in *Physics of Defects*, edited by R. Balian *et al.* (North-Holland Publishing Company, Amsterdam, 1981), pp. 715–755.
[32]I. Szleifer, D. Kramer, A. Ben-Shaul, W. M. Gelbart, and S. A. Safran, "Molecular theory of curvature elasticity in surfactant films," J. Chem. Phys. **92**, 6800–6817 (1990).
[33]G. Gompper and S. Klein, "Ginzburg–Landau theory of aqueous surfactant solutions," J. Phys. II France **2**, 1725–1744 (1992).
[34]A. Grafmüller, J. C. Shillcock, and R. Lipowsky, "The fusion of membranes and vesicles-pathway and energy barriers form dissipative particle dynamics," Biophys. J. **96**, 2658–2675 (2009).
[35]R. Lipowsky, "Coupling of bending and stretching deformations in vesicle membranes," Adv. Colloid Interface Sci. **208**, 14–24 (2014).
[36]R. Groot and P. Warren, "Dissipative particle dynamics: Bridging the gap between atomistic and mesoscopic simulation," J. Chem. Phys. **107**, 4423–4435 (1997).
[37]L. Gao, J. Shillcock, and R. Lipowsky, "Improved dissipative particle dynamics simulations of lipid bilayers," J. Chem. Phys. **126**, 015101 (2007).
[38]J. Rowlinson and B. Widom, *Molecular Theory of Capillarity* (Clarendon Press, Oxford, 1989).
[39]D. Marsh, *CRC Handbook of Lipid Bilayers* (CRC Press, Boca Raton, 1990).
[40]A. Imparato, J. Shillcock, and R. Lipowsky, "Shape fluctuations and elastic properties of two-component bilayer membranes," Europhys. Lett. **69**, 650–656 (2004).
[41]A. Imparato, "Surface tension in bilayer membranes with fixed projected area," J. Chem. Phys. **124**, 154714 (2006).
[42]J. Stecki, "Size dependence, stability, and the transition to buckling in model reverse bilayers," J. Chem. Phys. **125**, 154902 (2006).
[43]J. Neder, B. West, P. Nielaba, and F. Schmid, "Coarse-grained simulations of membranes under tension," J. Chem. Phys. **132**, 115101 (2010).
[44]O. Farago, "Mechanical surface tension governs membrane thermal fluctuations," Phys. Rev. E **84**, 051914 (2011).
[45]R. Lipowsky and S. Grotehans, "Renormalization of hydration forces by collective protrusion modes," Biophys. Chem. **49**, 27–37 (1993).
[46]G. Brannigan and F. L. H. Brown, "A consistent model for thermal fluctuations and protein-induced deformations in lipid bilayers," Biophys. J. **90**, 1501–1520 (2006).
[47]L. D. Landau and E. M. Lifshitz, *Theory of Elasticity* (Pergamon Press, New York, 1986).
[48]U. Seifert, K. Berndl, and R. Lipowsky, "Shape transformations of vesicles: Phase diagram for spontaneous curvature and bilayer coupling model," Phys. Rev. A **44**, 1182–1202 (1991).
[49]J. B. Fournier, "On the stress and torque tensors in fluid membranes," Soft Matter **3**, 883–888 (2007).
[50]See supplementary material at http://dx.doi.org/10.1063/1.4906149 for the three figures, S1–S3.
[51]R. Lipowsky, "Domains and rafts in membranes-hidden dimensions of self-organization," J. Biol. Phys. **28**, 195–210 (2002).
[52]R. Lipowsky, "Remodelling of membrane compartments: Some consequences of membrane fluidity," Biol. Chem. **395**, 253–274 (2014).
[53]J. Agudo-Canalejo and R. Lipowsky, "Two critical particle sizes for the engulfment of nanoparticles by biomembranes and vesicles" (unpublished).
[54]J. Shillcock and R. Lipowsky, "Visualizing soft matter: Mesoscopic simulations of membranes, vesicles, and nanoparticles," Biophys. Rev. Lett. **2**, 33–55 (2007).
[55]T. Yue and X. Zhang, "Molecular understanding of receptor-mediated membrane responses to ligand-coated nanoparticles," Soft Matter **7**, 9104–9112 (2011).
[56]T. Yue and X. Zhang, "Cooperative effect in recepctor-mediated endocytosis of multiple nanoparticles," ACS Nano **6**, 3196–3205 (2012).
[57]H. Ding and Y. Ma, "Interactions between Janus particles and membranes," Nanoscale **4**, 1116–1122 (2012).
[58]I. Salib, X. Yong, E. J. Crabb, N. M. Moellers, G. T. McFarlin IV, O. Kuksenok, and A. C. Balazs, "Harnessing fluid-driven vesicles to pick up and drop off Janus particles," ACS Nano **7**, 1224–1238 (2013).
[59]R. Dimova and R. Lipowsky, "Lipid membranes in contact with aqueous phases of polymer solutions," Soft Matter **8**, 6409–6415 (2012).

This article is copyrighted as indicated in the article. Reuse of AIP content is subject to the terms at: http://scitation.aip.org/termsconditions. Downloaded to IP: 141.14.232.254 On: Tue, 03 Feb 2015 17:28:05